

Measuring and Modeling Chloride-Hydroxyl Exchange in the Guinea-Pig Ventricular Myocyte

S. A. Niederer,^{*,†} P. Swietach,^{*} D. A. Wilson,^{*} N. P. Smith,[†] and R. D. Vaughan-Jones^{*}

^{*}Burdon Sanderson Cardiac Science Centre, Department of Physiology, Anatomy and Genetics, and [†]Computational Laboratory, University of Oxford, Oxford, United Kingdom

ABSTRACT Protons are powerful modulators of cardiac function. Their intracellular concentration is regulated by sarcolemmal ion transporters that export or import H^+ -ions (or their ionic equivalent: HCO_3^- , OH^-). One such transporter, which imports H^+ -equivalents, is a putative Cl^-/OH^- exchanger (CHE). A strong candidate for CHE is SLC26A6 protein, a product of the SLC26A gene family of anion transporters, which has been detected in murine heart. SLC26A6 protein is suggested to be an electrogenic $1Cl^-/2OH^-$ ($2HCO_3^-$) exchanger. Unfortunately, there is insufficient characterization of cardiac CHE against which the properties of heterologously expressed SLC26A6 can be matched. We therefore investigated the proton, Cl^- , and voltage dependence of CHE activity in guinea-pig ventricular myocytes, using voltage-clamp, intracellular pH fluorescence, and mathematical modeling techniques. We find that CHE activity is tightly regulated by intracellular and extracellular pH, is voltage-insensitive over a wide range (± 80 mV), and displays substrate dependence suggestive of electroneutral $1Cl^-/1OH^-$ exchange. These properties exclude electrogenic SLC26A6 as sole contributor to CHE. Either the SLC26A6 product in heart is electroneutral, or CHE comprises at least two transporters with oppositely balanced voltage sensitivity. Alternatively, CHE may comprise an H^+-Cl^- cotransport system, which cannot be distinguished kinetically from an exchanger. Irrespective of ionic mechanism, CHE's pH sensitivity helps to define resting intracellular pH, and hence basal function in the heart.

INTRODUCTION

In the heart, intracellular pH (pH_i) exerts a major influence on cellular processes such as Ca_i^{2+} signaling (1), contraction (2) and electrical excitability (3). It is no surprise, therefore, that cardiac myocytes possess a sophisticated pH_i regulatory system. This comprises powerful cytoplasmic buffers and sarcolemmal ion-transport proteins. Among the latter, Na^+/H^+ exchange and $Na^+-HCO_3^-$ cotransport extrude excess acid from the myocyte, while Cl^-/HCO_3^- exchange and Cl^-/OH^- exchange extrude excess base (4). A sarcolemmal lactic acid transporter is also recruited in response to enhanced anaerobic metabolism (5). Under normal physiological conditions, the regulatory system maintains pH_i at a steady-state value of ~ 7.2 .

Of the various ion transporters involved in cardiac pH_i regulation, least is known about Cl^-/OH^- exchange. It was first identified functionally in guinea-pig myocytes as an H^+ -equivalent influx transporter that reduces pH_i (6,7). Subsequent work has also implicated its presence in rat (unpublished) and rabbit ventricular myocytes (8). Its activity is Cl^- -dependent, Na^+ -independent, and is activated by low extracellular pH (pH_o) and high pH_i . H^+ -equivalent transport through the carrier seems to be unaffected by the removal of CO_2/HCO_3^- , or by the addition of 0.5 mM 4,4'-diisothiocyanatostilbene-2,2'-disulfonic acid (DIDS), a Cl^-/HCO_3^- exchange inhibitor (6,7,9). These results appear to rule out known myocardial products of the Anion Exchange (AE) gene family (the

SLC4A family) as candidates for CHE, all of which are DIDS-sensitive and transport HCO_3^- (10). An independent Cl^-/OH^- exchanger (CHE) or, alternatively, an H^+-Cl^- cotransporter, has therefore been proposed. Recently, protein and mRNA products of the SLC26 superfamily, most notably SLC26A6, have been identified in murine myocardium (11). When transfected into HEK293 cells, the protein product mediates both Cl^-/HCO_3^- and Cl^-/OH^- exchange with relatively low sensitivity to DIDS, suggesting it may account for CHE activity in heart.

There has been no extensive characterization of the kinetic transport properties of cardiac CHE. Without this, a comparison cannot be made with the properties of heterologously expressed candidate transporters. In this work, we have therefore monitored H^+ -equivalent flux through CHE in guinea-pig ventricular myocytes loaded with the pH-sensitive fluorescent dye, carboxy-seminaphtharhodafleur-1 (carboxy-SNARF-1). We have quantified the dependence of ion transport on extracellular Cl^- concentration, and on pH_o and pH_i . We have also examined the effects of manipulating membrane potential on CHE kinetics, in view of a recent debate on the voltage sensitivity and electrogenicity of some SLC26A gene products, with reports both for (12–14) and against (15) electrogenicity.

Having characterized the kinetic properties of CHE, we have used computational modeling to explore the underlying mechanism. Such an approach, when applied previously to epithelial brush-border membranes, suggested that H^+-Cl^- cotransport rather than Cl^-/OH^- exchange was the more likely ionic arrangement (16). We have investigated if such a distinction can be made for the system in heart. We have also

Submitted August 2, 2007, and accepted for publication November 2, 2007.

Address reprint requests to Richard D. Vaughan-Jones, Tel.: 00-44-1865-272451; E-mail: richard.vaughan-jones@dpag.ox.ac.uk.

Editor: David S. Weiss.

© 2008 by the Biophysical Society
0006-3495/08/03/2385/19 \$2.00

doi: 10.1529/biophysj.107.118885

analyzed our data for evidence of allosteric regulation of CHE by pH_i and pH_o . Results of experiments and modeling demonstrate that CHE is specialized to import acid into the cardiac myocyte, in a voltage-insensitive but tightly proton-controlled manner. Candidate transporters that may underpin these properties are considered.

METHODS

Isolation of guinea-pig ventricular myocytes

The procedures used in the isolation process have been described previously (17). Briefly, after cervical dislocation, hearts were excised from female albino guinea-pigs (350–450 g) and perfused via a modified Langendorff method. Single ventricular myocytes were isolated using both enzymatic and mechanical dispersion (for some experiments, we used 0.7 mg/ml collagenase, Type I or II (Worthington Biochemical, Reading, UK) and 0.04 mg/ml protease (Sigma, St. Louis); for others, we used Blendzyme III (Roche Diagnostics, Burgess Hill, UK). The cells were suspended in 4-(2-hydroxyethyl)-1-piperazineethanesulfonic acid (HEPES) buffered Dulbecco's modified Eagle's medium and left at room temperature until use. Myocytes that displayed a rod shape and calcium tolerance were used in the study.

pH_i measurements

The pH_i of single isolated myocytes was measured using carboxy-SNARF-1, a dual-emission, pH_i -sensitive fluorophore. Cells were loaded by incubation in a 10–20 μM solution of carboxy-SNARF-1-AM ester at room temperature for 5–10 min. Carboxy-SNARF-1 loaded in individual cells was excited at 540 ± 12 nm and fluorescence emission was measured simultaneously at 590 ± 5 and 640 ± 5 nm using an inverted microscope (Diaphot; Nikon, Kingston upon Thames, UK) adopted for epifluorescence. The signals were digitized at 0.5 kHz (CED 1401+). The SNARF emission ratio (590 nm/640 nm) was calculated and converted to a pH_i value using calibration data, obtained by superfusing 145 mM K^+ -containing solutions at pH 8.5, 7.5, 6.5, and 5.5, containing 10 μM nigericin, as described by Thomas et al. (18).

Solutions

Experiments were performed using nominally HCO_3^- -free, HEPES-buffered Tyrode solutions containing (mM): 140 NaCl, 1.0 MgCl_2 , 4.5 KCl, 2.0 CaCl_2 , 11 glucose, and 20 HEPES ($\text{pK}_a = 7.5$) for pH values 6.8, 7.4, and 7.8. When required, the solution contained 20 mM 3-[4-(2-Hydroxyethyl)-1-piperazinyl]propanesulfonic acid (HEPPS) ($\text{pK}_a = 8.0$) for pH 8.4, or 20 mM 2-(*N*-morpholino) ethanesulfonic acid (MES) ($\text{pK}_a = 6.1$) for pH 6.4 and 6.2. Cl^- -free Tyrode solutions contained (mM): 140 Na-gluconate, 4.5 K-gluconate, 4.0 Ca-gluconate, 1.0 Mg-gluconate, 11 glucose, and 20 HEPES, MES, or HEPPS. When acetate was added to solutions, an equimolar amount of anion (either Cl^- or gluconate) was omitted. In the experiments performed to determine the Cl_o^- -dependence, equimolar substitutions were performed to give the required concentration of $[\text{Cl}_o^-]$ (1.4, 14, and 98 mM), while osmolality was maintained at 300 mOsm/kg (measured with an osmometer; Micro Instruments, Witney, UK). In most experiments, when measurements of acid-equivalent influx were made, 30 μM HOE 694 (an NHE inhibitor) was included in the superfusates, except at pH_o 8.4, when 300 μM HOE 694 was added, as the drug is only active in the protonated form ($\text{pK} \sim 8.2$ base on a derivative, amiloride (19)).

Experimental protocols

The standard experimental protocol for studying CHE activity (as demonstrated in Fig. 1) consisted of baseloading the cell using a 3–4 min acetate

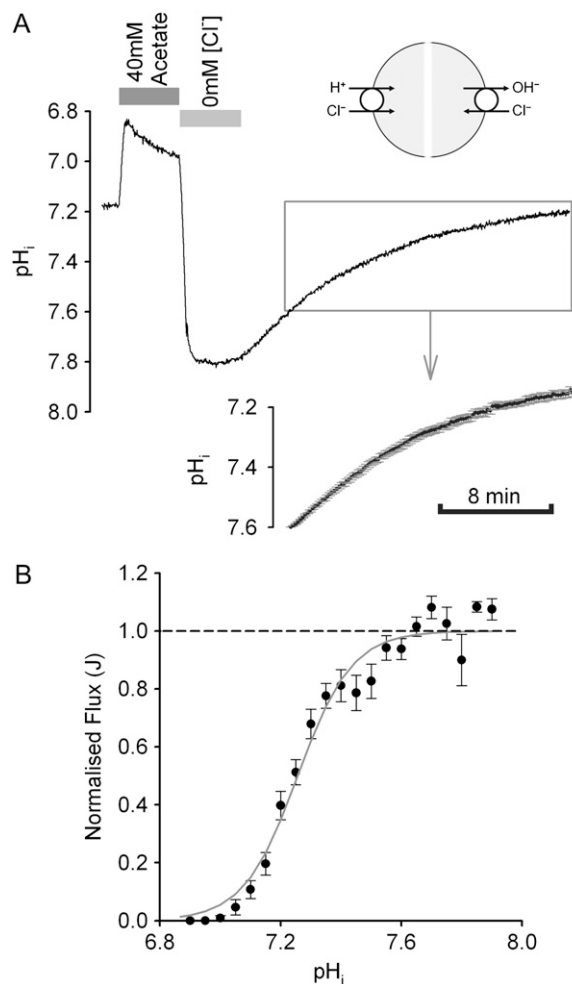


FIGURE 1 Stimulating CHE: recovery from alkaline pH_i . (A) Experimental protocol illustrating the acetate prepulse technique, used to baseload a guinea-pig ventricular myocyte superfused with Cl^- -free HEPES-buffered Tyrode's solution. The myocyte is exposed transiently (4 min) to 40 mM sodium acetate. Readmitting Cl_o^- then reactivates CHE, permitting pH_i to recover to control levels. The upper inset (cartoon) illustrates possible ionic mechanisms. Whole-cell intracellular pH recorded using intracellular, ratiometric SNARF fluorescence. The lower inset shows a portion of the pH_i recovery, averaged over the pH_i range 7.6–7.2 ($n = 15$ experiments). (B) Recovery rates for pH_i have been converted to values for H^+ -equivalent influx (see Methods), and plotted versus pH_i in the range 7.8–7.0 ($n = 9$ –15 measurements for each point). H^+ -equivalent influx has been normalized to the peak flux, estimated by fitting the data with a Hill curve. The best-fit (shaded curve) is described by a Hill coefficient of 4.8 and a pK of 7.25.

prepulse (40–80 mM, depending on the desired magnitude of post-acetate alkalosis). Upon acetate removal, cells were perfused with a Cl^- -free solution to maintain the intracellular baseload. Readdition of Cl_o^- reactivated CHE, resulting in a recovery of pH_i back to control levels. Experiments were performed when cells were superfused with air-equilibrated solution (i.e., nominally CO_2 -free conditions). When perfusates devoid of CO_2 were required, they were equilibrated with 100% O_2 in loosely stoppered glass flasks, and solution was led to the superfusion chamber through double-sleeved silastic tubing, with 100% O_2 flowing through the double-sleeved space. The volume above the superfusion chamber was surrounded by a 10-cm-high Perspex collar, also filled with flowing 100% O_2 . The ability of the perfusion system to exclude a selected atmospheric gas was initially

tested by switching the perfusate to 100% N₂-equilibrated Tyrode's, and measuring the fall of PO₂ in the solution flowing through the chamber, using a miniature O₂-electrode (PreSens, Regensburg, Germany). PO₂ was reduced to ~0.5 Torr in ~15 min. This implied that atmospheric PCO₂ in a superfusate (nominally 0.03% in air-equilibrated solution) would be reduced by nearly 300-fold (to 0.0001%), when 100% O₂-equilibrated solutions were flowing through the chamber.

Calculation of net sarcolemmal H⁺-equivalent influx

Net H⁺-equivalent influx through CHE was estimated from the accompanying fall of p*H*_i. Net acid influx (*J*_{H⁺}ⁱ) was computed using the equation

$$J_{\text{H}}^{\text{i}} = \beta_{\text{int}}(\text{pH}_i) \times \frac{d\text{pH}_i}{dt}, \quad (1)$$

where β_{int} (intrinsic buffering power) is the H⁺-ion buffering capacity in the cell, and is a function of p*H*_i, as measured previously (20). In most experiments, as described above, CHE activity was initiated by re-adding Cl_o⁻ after initially baseloading the cell under Cl_o⁻-free conditions. In some experiments, CHE activity was estimated when Cl_i⁻ concentration was close to zero (see, e.g., Fig. 4 and Fig. 5 C). In these cases, the value for *dpH_i/dt* was obtained from the initial p*H*_i change (linear regression to first 30s of p*H*_i change) measured after readdition of Cl_o⁻. In other experiments, H⁺-equivalent influx was measured at different times after Cl_o⁻ readdition. In these latter cases (see, e.g., Fig. 1 and Fig. 5 B), *dpH_i/dt* was measured at different successive values of p*H*_i during CHE activity. This was done by piecewise fitting of the p*H*_i timecourse, measuring the *dpH_i/dt* gradient every 5 s, and then interpolating the flux to the desired p*H*_i (taken as the midpoint of the p*H*_i change).

Averaged data are presented as mean ± SE, where *n* = number of observations.

Electrophysiological measurements

Electrophysiological measurements were made with whole-cell, ruptured-patch pipettes, made of borosilicate capillary glass (No. 8250; Dow Corning, Corning, NY) with resistance typically 1.5 MΩ when backfilled. Filling solutions contained 15 mM NaCl, 110 mM K-aspartate, 5 mM KCl, 5 mM MgCl₂, 14 mM HEPES (to match the buffering capacity of intracellular mobile buffer (21)), pH-adjusted to 7.15 with 2 M KOH. Voltage-clamp control was provided by a model No. 200B system with a model No. CV203BU cooled headstage (Axopatch, Axon Instruments, Union City, CA). Membrane potential (*V*_m) and membrane current (*I*_m) were filtered at 5 kHz, digitized at 10–20 kHz with a 16-bit A/D converter (model No. 1322A; Axon Instruments), and analyzed using pCLAMP 8 software (Axon Instruments). The reference electrode was a flowing 3 M KCl bridge for experiments involving changes in bath Cl⁻, and an Ag-AgCl pellet was used when Cl_o⁻ was maintained at a constant concentration. Cells were held initially at -80 mV and then clamped to +80 mV for 2–4 min. Bathing solutions contained 0.5 mM BaCl₂ to block inward *I*_{K1}, and 10 μM nifedipine to reduce Ca²⁺ entry that may subsequently affect p*H*_i (22). Cell p*H*_i was simultaneously measured using carboxy-SNARF-1, as described above. The reversal potential for electrogenic CHE (*E*_{CHE}) transporting *n* H⁺-equivalent and *m* Cl⁻ ions across the membrane was calculated using the formula

$$E_{\text{CHE}} = \frac{RT}{(n-m)F} \ln \left(\left(\frac{[\text{Cl}^-]_o}{[\text{Cl}^-]_i} \right)^m \left(\frac{[\text{H}^+]_o}{[\text{H}^+]_i} \right)^n \right), \quad (2)$$

where *R*, *T*, and *F* are the gas constant, temperature, and Faraday's constant, respectively. In the calculation, we have assumed constant [Cl⁻]_i or allowed [Cl⁻]_i to increase as a result of CHE activity.

Modeling methods

In this study, we derive transporter models to elucidate the currently unknown modality of the cardiac CHE carrier. The model rate constants for a given cycle are constrained via thermodynamic principles, where the products of the forward and backward rates for a given cycle are equal at equilibrium. The steady-state fluxes are calculated using rapid equilibrium assumptions for ion binding and unbinding. The transitions between intracellular and extracellular facing conformations are assumed to take place more slowly than ion binding events, and hence the forward and backward rates are represented explicitly. Voltage variation is assumed to be small during experiments (removal and readdition of Cl_o⁻ affects membrane potential of cardiac tissue by only a few mV (23)) allowing the voltage dependence of any model parameter to be assumed constant.

Starting with simple electroneutral transporter models (six-state models), we proceed to more complex arrangements incorporating, for example, multiple substrate binding sites (eight-state models), an allosteric H⁺ modifier site, and a putative electrogenic transport stoichiometry (twelve-state models). In each case, we assess the ability of the model to reproduce the experimental results. The models are described in Results, and the governing equations are provided in the Appendix.

RESULTS

Measuring CHE activity

Fig. 1 A illustrates the experimental protocol for activating CHE. An isolated ventricular myocyte was superfused with HEPES-buffered Tyrode's, nominally free of CO₂/HCO₃⁻ buffer. Prepulsing the cell with 40 mM extracellular acetate induced an intracellular baseload. In the absence of extracellular Cl⁻ (replaced by gluconate), p*H*_i stabilized at ~7.8. Readdition of Cl_o⁻ then prompted an intracellular acidification, consistent with Cl⁻-influx coupled to OH⁻ efflux on a Cl⁻/OH⁻ exchange transporter (or, alternatively, HCl influx on an H⁺-Cl⁻ cotransporter). For convenience, we refer to this as an H⁺-equivalent influx on CHE. Several experimental records from different cells have been averaged in the inset to Fig. 1 A, demonstrating the monotonic intracellular acidification. H⁺-equivalent influx (*J*_{H⁺}ⁱ) was estimated from individual p*H*_i timecourses (see Methods), measured over a range of p*H*_i values. Fig. 1 B shows average H⁺-equivalent influx, normalized to the maximal flux estimated from the best-fitting Hill curve. The data shows that flux increased steeply at p*H*_i values above 7.0 and saturated at ~7.6. The stimulation of CHE activity by a rise of p*H*_i is consistent with previous reports (4,7).

CHE activity is not dependent on HCO₃⁻ availability

CHE activity is clearly evident when myocytes are superfused with CO₂/HCO₃⁻-free Tyrode's to block Cl⁻/HCO₃⁻ exchange activity ((6,9); see also Fig. 1). Residual Cl⁻/HCO₃⁻ exchange may persist, however, because of HCO₃⁻ contamination, caused by the hydration of atmospheric or metabolically produced CO₂. A previous attempt has been made to remove these sources of CO₂ (9), but specific effects on Cl⁻-dependent H⁺-equivalent influx were not examined.

Fig. 2 A illustrates an experiment performed using HEPES-buffered superfusates. A myocyte was baseloaded (acetate prepulse) in Cl^- -free solution, while pH_o was reduced to 6.4. Re-adding Cl_o^- (solid trace) prompted a robust intracellular acidification via CHE. A Cl^- -activated acidification occurred (shaded trace, and see Fig. 2 B) even when the superfusate contained 10 μM rotenone (to inhibit metabolic CO_2 production) and was saturated with 100% O_2 (to remove atmospheric CO_2 -contamination). Mean Cl^- -activated acid influx was also quantified (Fig. 2 C) when 3 mM cyanide was used instead of rotenone (in this case pH_o was adjusted to 7.8 rather than 6.4). The cause of the higher background, Cl^- -independent acid-loading observed in these latter experiments (Fig. 2 C, column 2) was not established, but it may reflect an ability of HCN to act as a membrane-permeant proton carrier. Cl^- -activated acid influx, however, was unaffected by cyanide (Fig. 2 C, column 4), indicating that CHE

activity is not reliant on residual HCO_3^- availability and must be caused by OH^- -ion efflux or H^+ -ion influx.

Electrogenic CHE?

Although protein products of the SLC4A anion exchange gene family (AE) are electroneutral transporters (10), some anion exchange products of another family, SLC26A, are thought to be electrogenic and voltage-sensitive (12–14). Depending on the isoform, they exchange two HCO_3^- or OH^- ions for each Cl^- ion (e.g., SLC26A6; (13,14)), or two Cl^- ions for each OH^- or HCO_3^- (e.g., SLC26A3; (13,14)). We explored the possible voltage sensitivity of cardiac CHE by manipulating membrane potential under voltage-clamp (ruptured patch) conditions. Fig. 3 shows one such experiment. Membrane potential was clamped initially at -80 mV, while pH_i was measured simultaneously. CHE was then

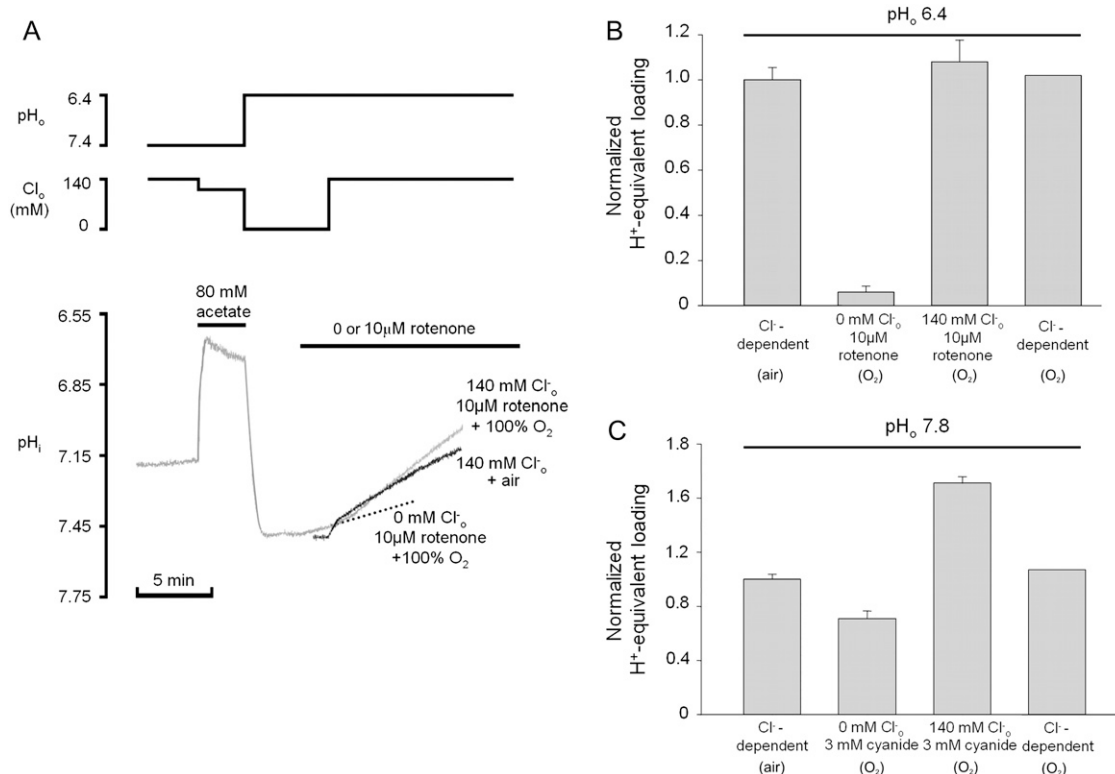


FIGURE 2 HCO_3^- independence of CHE activity. (A) Shaded trace: a guinea-pig myocyte is baseloaded (80 mM acetate prepulse) during superfusion with HEPES-buffered, air-equilibrated solution containing 30 μM HOE 694 (to inhibit NHE). On removal of acetate, cell is exposed to Cl^- -free solution of pH 6.4, and then additionally to 100% O_2 and 10 μM rotenone (to create CO_2 -free conditions). The pH_i acidifies slowly (dashed trace). Readdition of 140 mM Cl_o^- (to reactivate CHE) stimulates a more rapid acidification. (Solid trace) Different experiment, showing Cl_o^- readdition, when superfusates are air-equilibrated, contain 30 μM HOE 694, and lack rotenone. Note that Cl^- -dependent acidification is comparable in the two traces. (B) Cl^- -dependent H^+ -equivalent loading in air-equilibrated solutions, estimated from pH_i -acidification rates; (column 1) H^+ -equivalent loading in Cl^- -free, CO_2 -free conditions; (column 2) H^+ -equivalent loading after Cl_o^- readdition in CO_2 -free conditions; and (column 3) Cl^- -dependent H^+ -equivalent loading in CO_2 -free conditions (column 3 minus column 2) ($n = 6$). H^+ -equivalent loading in O_2 was sampled at pH_i 7.4, and normalized to the control Cl^- -dependent loading measured in air. (C) Cl^- -dependent H^+ -equivalent loading is similar in air and in O_2 -equilibrated, CN^- -containing conditions (30 μM HOE 694 present in superfusates); loading rates sampled at pH_i 7.4, and normalized to Cl^- -dependent rate measured in CN^- -free, air-equilibrated conditions. A quantity of 3 mM NaCN was added to a baseloaded myocyte bathed in Cl^- -free 100% O_2 -equilibrated solution of pH 7.8 (column 2); Cl_o^- readdition prompted a larger H^+ -equivalent loading (column 3); Cl^- -dependent H^+ -equivalent loading in 100% O_2/CN^- (column 4) is comparable to Cl^- -dependent loading measured in CN^- -free, air-equilibrated conditions (column 1) ($n = 6$).

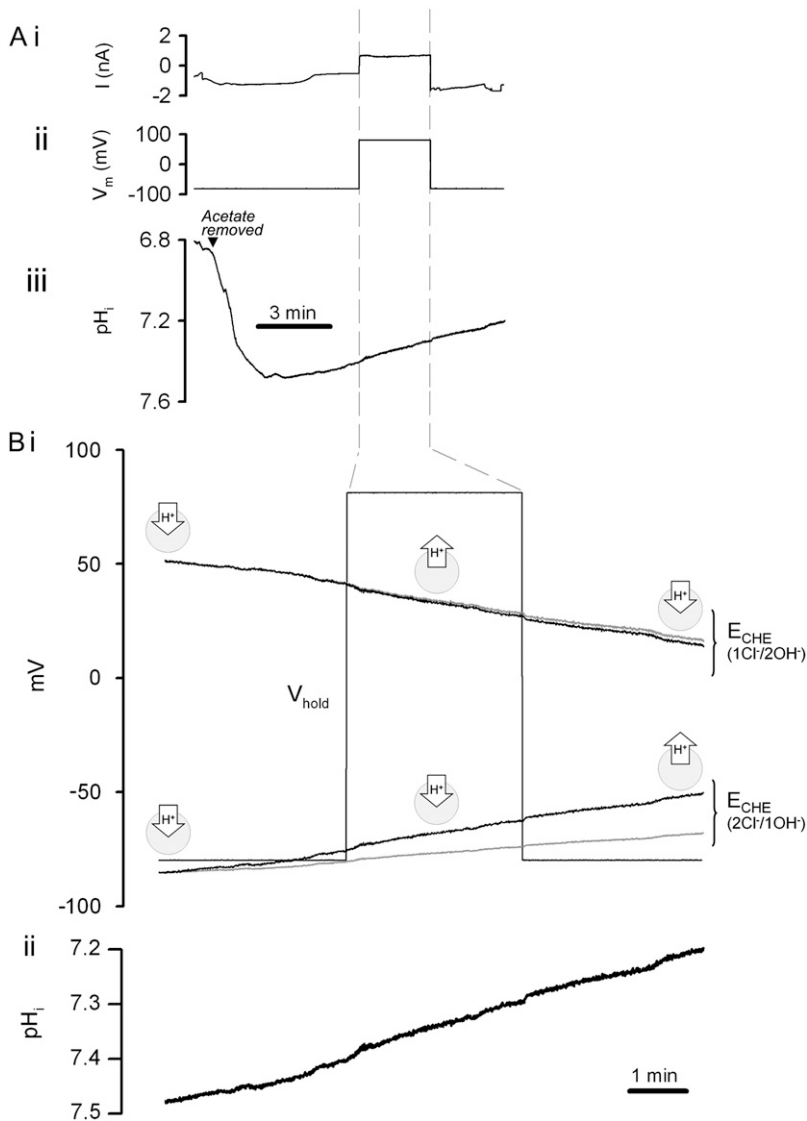


FIGURE 3 Voltage independence of CHE activity. (A) A guinea-pig myocyte, in a nominally CO_2 -free HEPES-buffered Tyrode solution, was voltage-clamped in whole-cell, ruptured-patch configuration, while pH_i was monitored simultaneously. The myocyte was baseloaded by an 8 min prepulse with 40 mM acetate. During recovery of pH_i from the baseload, holding potential (V_{hold}) was depolarized from -80 mV to $+80$ mV for a period of 3 min. (i) Current injected into myocyte, (ii) membrane potential, (iii) pH_i . (B). (i) Timecourse of holding potential (V_{hold}) and predicted reversal potentials (E_{CHE}) for two putative forms of electrogenic CHE transport, $2Cl^-/1OH^-$ and $1Cl^-/2OH^-$, plotted assuming constant $[Cl^-]_i$ of 30 mM, equal to pipette-filling solution $[Cl^-]$ (shaded trace), or assuming that $[Cl^-]$ rises over time from 30 mM, due to CHE activity (solid trace); $[Cl^-]_i$ rising by 2.6 and 10.6 mM for $Cl^-/2OH^-$ and $2Cl^-/1OH^-$, respectively. Inward and outward H^+ -flux icons represent thermodynamically predicted direction of carrier activity. (ii) pH_i recovery from alkaline pH_i , replotted at higher amplification from panel Aiii, showing lack of effect of membrane potential on timecourse of pH_i recovery (compare this to the direction of pH_i change expected from individual electrogenic transporters, see icons). Similar results were obtained in four other experiments.

stimulated by alkalinizing the cell (by acetate prepulse), whereupon pH_i started to recover back to control levels. The membrane potential was then depolarized to $+80$ mV for 3 min (Fig. 3 Bi). Superimposed on the membrane potential trace are the reversal potentials (E_{CHE}) expected for a $1Cl^-/2OH^-$ and a $2Cl^-/1OH^-$ exchanger (see Methods). Note that the values for E_{CHE} are predicted to vary over time in accordance with the changes of pH_i . Note also that, at different times during the experiment, the electrochemical driving force ($V_m - E_{CHE}$) acting on each putative electrogenic carrier would have been reversed (i.e., at different times, the holding potential was positive or negative to a transporter's reversal potential), which should terminate or even reverse carrier activity. Despite this, there was no detectable effect on the rate or direction of recovery of pH_i (Fig. 3 Bii). Similar results were obtained in four other experiments. We conclude that cardiac CHE behaves functionally as an electroneutral, voltage-insensitive system. CHE activity cannot be described

solely by a $1Cl^-/2OH^-$ or a $2Cl^-/1OH^-$ transporter. We return to this point in the Discussion.

$[Cl^-]_o$ -dependence of CHE activity

Fig. 4 Ai illustrates pH_i recovery from a baseload (induced by 80 mM acetate prepulse), after readdition of 140 mM Cl^-_o . Fig. 4 Aii shows that, in a separate experiment, a slower recovery was induced by readdition of 14 mM Cl^-_o . Fig. 4 B pools data from several experiments where various concentrations of Cl^-_o (0–140 mM) were tested. To remove effects of NHE, 30 μ M HOE 694 was added to all superfusates. In each case, initial H^+ -equivalent influx was estimated immediately after the addition of Cl^-_o , when Cl^-_i concentration is close to zero (see Methods). Initial Cl^- -activated H^+ -equivalent influx, computed at a common pH_i of 7.5–7.55, was a saturating function of $[Cl^-]_o$ (open squares). In other experiments, pH_o was reduced to 6.4 and then Cl^-_o was re-added. In

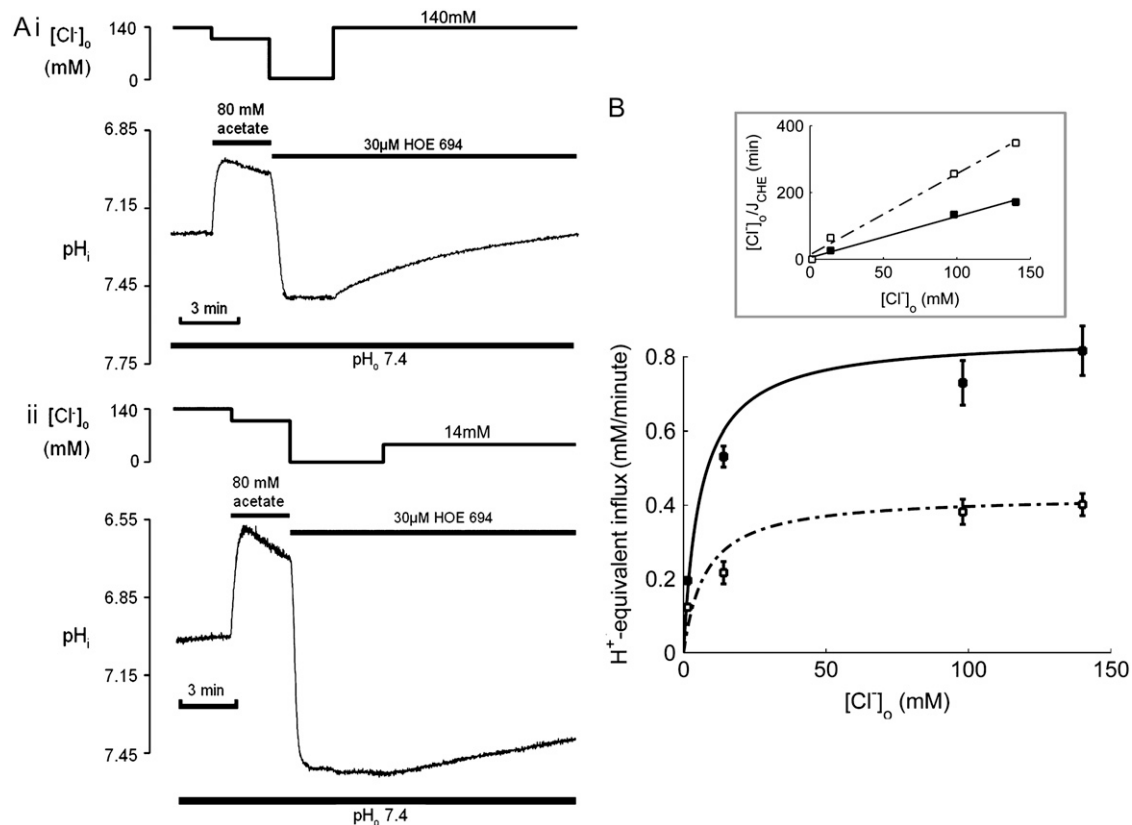


FIGURE 4 $[\text{Cl}^-]_o$ -dependence of CHE activity. (A) Recovery of pH_i was measured after readdition of (i) 140 mM or (ii) 14 mM Cl^- , after an acetate prepulse performed to baseload a guinea-pig myocyte in a nominally CO_2 -free HEPES-buffered Tyrode solution. HOE 694 ($30 \mu\text{M}$) was included to block Na^+ - H^+ exchange during Cl^- -activated pH_i recovery. Superfusate pH_o was maintained at 7.4. (B) The timecourses of pH_i recovery were converted to H^+ -equivalent influx computed at $\text{pH}_i = 7.5\text{--}7.55$, and plotted as a function of $[\text{Cl}^-]_o$ (1.4, 14, 100, 140 mM). Measurements ($n = 6$) were performed on experiments at pH_o 7.4 (open symbols) or 6.4 (solid symbols). Flux values are derived from the initial rate of recovery of pH_i , when $[\text{Cl}^-]_i$ is close to zero. Data were best-fitted with Hill curves with cooperativity 0.76 and 0.85 for pH_o 7.4 and 6.4, respectively. (Inset) A Hanes plot demonstrates that changing pH_o has a significant effect on V_{max} (slope⁻¹) and only a modest effect on K_m (intercept) for Cl_o^- .

these cases, initial Cl^- -activated H^+ -equivalent influx, again taken at a common pH_i of 7.5–7.55, was still a saturating function of $[\text{Cl}^-]_o$, but maximal flux (V_{max}) was significantly larger. A Hanes Plot of the data (Fig. 4 B, inset) demonstrated that reducing pH_o from 7.4 to 6.4 had the principal effect of doubling V_{max} ($1/\text{slope}$) from 0.43 to 0.86 mM min^{-1} , compared with only a modest shift in K_m (y intercept = K_m/V_{max}) from 6 mM to 8 mM. Hill coefficients for flux activation by Cl_o^- were 0.76 ± 0.2 (pH_o 7.4) and 0.85 ± 0.1 (pH_o 6.4), suggesting no more than one binding site for Cl^- on the transporter.

Dependence on pH_i

Fig. 5 A shows sample traces superimposed from three experiments where CHE activation was recorded by re-adding Cl_o^- at three different pH_o values (6.4, 7.4, and 8.4). The lower the pH_o , the faster and larger the Cl^- -activated intracellular acidification. Further experiments showed that the changes of pH_i were greatly reduced when pH_o was altered in the absence of Cl_o^- (Fig. 5 A, inset), indicating a

Cl^- -independent H^+ -equivalent influx of -0.12 , 0.0 , and 0.23 mM min^{-1} , at pH_o 8.4, 7.4 and 6.4. In contrast, influx measured in the presence of Cl_o^- could be as large as 1.2 mM min^{-1} .

Data, averaged from several individual experiments, are plotted in Fig. 5 B, after subtracting the Cl^- -independent H^+ -equivalent influx. The Cl^- -dependent flux increased steeply with a rise of pH_i from 7.0 to 7.5 (compare with Fig. 1 B), displaying an apparent H_i^+ cooperativity of >3.0 (see Fig. 5 B, inset). This is reminiscent of the high cooperativity for H_i^+ activation of Na^+/H^+ exchange (NHE 1) (24), with the difference that, for CHE, intracellular H^+ ions appear to inhibit rather than stimulate the transporter. High H_i^+ cooperativity for NHE activation has been suggested to be caused by H_i^+ -binding to an allosteric modifier site(s), in addition to the transport site on the carrier protein. The curves drawn through the points in Fig. 5 B (main panel) have been fitted using allosteric models for CHE, described later in the Results. Reducing pH_o displaces the pH_i dependence of CHE activity to the left along the pH_i axis, to lower pH_i values (Fig. 5 B). Thus, the sensitivity of CHE to pH_i is modulated by

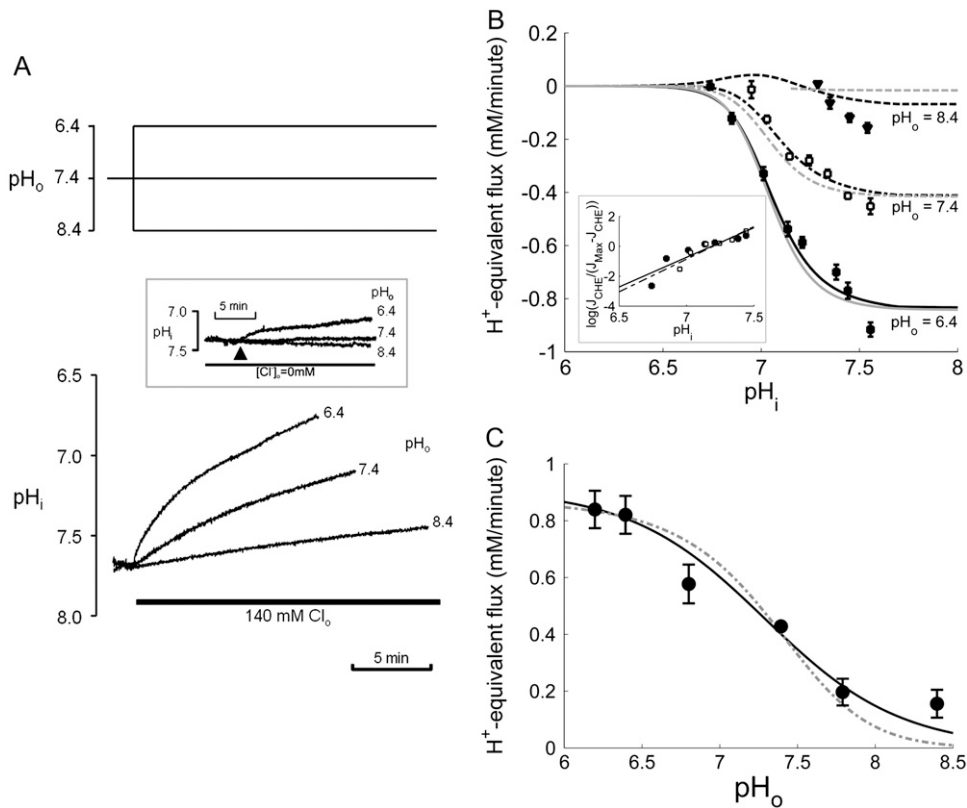


FIGURE 5 pH_i - and pH_o -dependence of CHE activity. (A) Recovery of pH_i was measured after readdition of 140 mM Cl^- at pH_o 6.4, 7.4, or 8.4, after an acetate prepulse performed to baseload a guinea-pig myocyte in a nominally CO_2 -free HEPES-buffered Tyrode's solution. Thirty-micrometers HOE 694 was included to block Na^+/H^+ exchange during Cl^- -activated pH_i recovery. (Inset) pH_i timecourses measured in the absence of Cl^- , at three pH_o values. The arrow indicates the time of the change of pH_o . (B) The timecourses of pH_i recovery were converted to H^+ -equivalent flux, calculated over the pH_i range 6.8–7.6 for pH_o 6.4 (solid squares), 7.4 (open squares), and 8.4 (solid triangles). Cl^- -independent flux was subtracted from the data. The data were fitted with models for electroneutral CHE (solid curves) or $1\text{Cl}^-/2\text{OH}^-$ electrogenic CHE (shaded curves). (Inset) a Hill plot of data measured at pH_o 7.4 (solid squares) and 6.4 (open squares) fitted with Hill coefficients of 4.37 and 3.97. (C) measurements of H^+ -equivalent influx plotted as a function of pH_o , estimated at a common pH_i of 7.69. The data were fitted with model of electroneutral CHE (solid curve) or $1\text{Cl}^-/2\text{OH}^-$ electrogenic CHE (dashed curve).

pH_o . In effect, reducing pH_o attenuates the inhibitory effect of intracellular H^+ ions on CHE activity.

Dependence on pH_o

Fig. 5 C shows H^+ -equivalent flux through CHE, plotted as a function of pH_o . Measurements of initial acid influx after Cl_o^- readdition were made (see Methods) at a common value of pH_i (~ 7.7). Reducing pH_o increased H^+ -equivalent influx, consistent with previous reports for CHE activity (6); the effect tended toward saturation at pH_o values of 6.2. Sensitivity to pH_o can be best described by an H^+ -binding curve with a Hill coefficient of 0.96 ± 0.11 , consistent with a single extracellular H^+ -binding site. There was no evidence for a high level of H_o^+ cooperativity, unlike that measured for H_i^+ . Sensitivity to pH_o displayed half-maximal activity at a value of ~ 7.25 , close to the physiological value of pH_o (7.4). Thus, in addition to intracellular pH (see above), extracellular pH will be a key determinant of CHE activity.

Kinetic models of CHE: Cl^-/OH^- exchange or H^+/Cl^- cotransport?

In the following sections, we use computational modeling to assess possible transporters that may underpin cardiac CHE activity. Initially, we ask if the H^+ -equivalent substrate can be identified unequivocally as an OH^- or an H^+ ion. To do

this, we explore the transport modalities illustrated in Fig. 6. The two modes are either a ping-pong Cl^-/OH^- exchanger (Fig. 6 Ai) or an H^+/Cl^- cotransporter (Fig. 6 Bi). For simplicity, we consider the case of an electroneutral system, as this is consistent with the voltage insensitivity of CHE (Fig. 3). The additional complexity of an allosteric H_i^+ -binding site is dealt with later. A six-state model represents the simplest scheme where, for an exchanger (Fig. 6 Aii), there is a single binding site on the internal or external configuration of the carrier, to which either a Cl^- or OH^- ion attaches while, for cotransport (Fig. 6 Bii), there is ordered Cl^- and H^+ -ion binding to separate sites. An eight-state model is more flexible: for an exchanger (Fig. 6 Aiii), it allows binding of Cl^- and OH^- to independent sites in both the inward and outward facing configurations, although translocation of only one ionic species (Cl^- or OH^-) is permitted at any time. For cotransport (Fig. 6 Biii), the eight-state model allows for random-order binding of H^+ and Cl^- ions. Details of the derivation of the eight-state model are given in the Appendix.

We demonstrate below that the experimental results shown in Fig. 4 B require a model with a minimum of eight states, and that such models cannot distinguish between OH^- or H^+ ion transport. Fig. 4 B quantified the Cl_o^- dependence of CHE activity. As those measurements were performed at a pH_i of ~ 7.5 , transport inhibition caused by H^+ binding to an intracellular allosteric modifier site would have been minimal

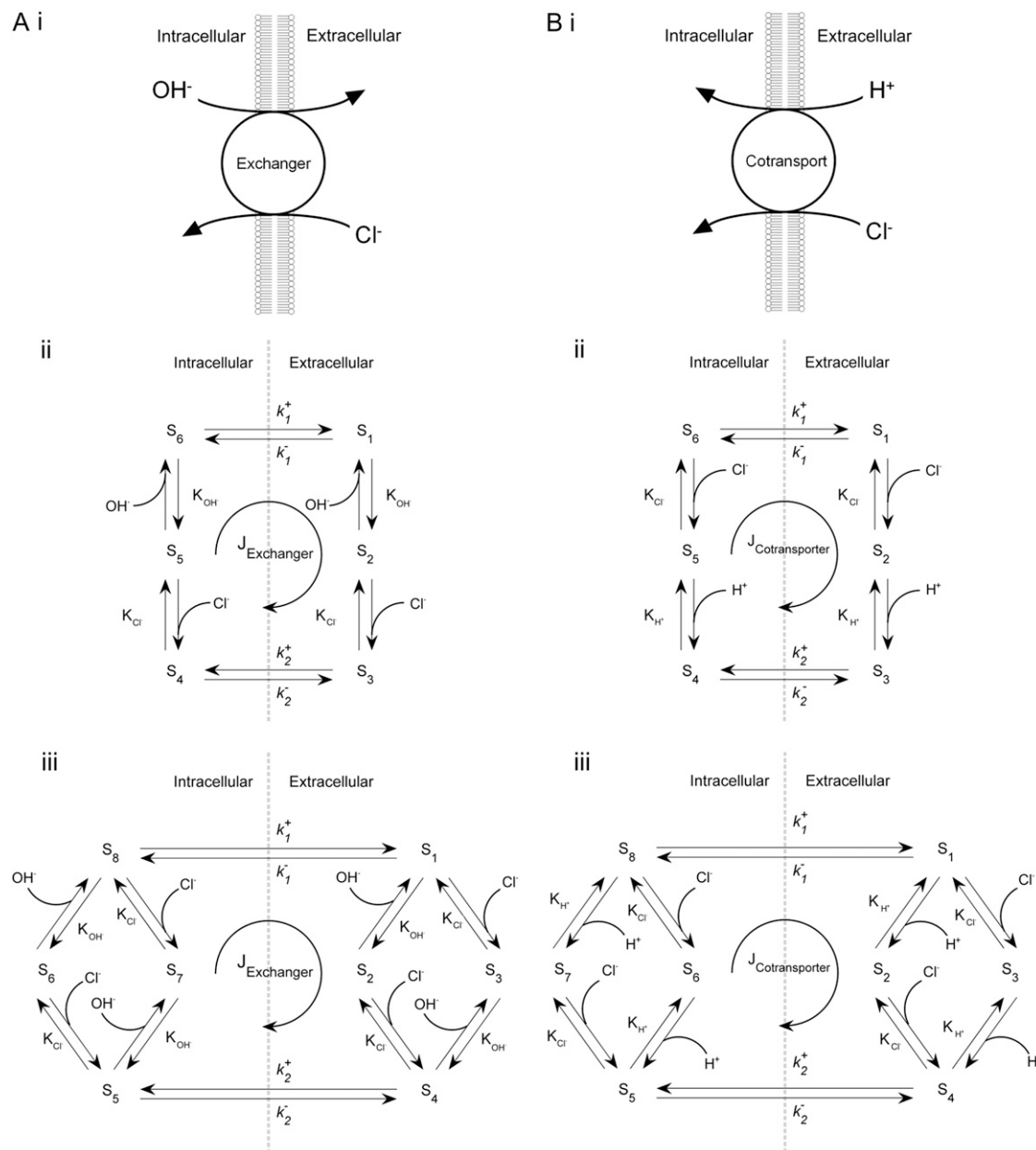


FIGURE 6 Schematic diagrams for six- and eight-state kinetic CHE models. Kinetic diagrams: Cl^-/OH^- exchanger models (A, left panels) and H^+-Cl^- cotransporter models (B, right panels). Cartoons for (Ai) Cl^-/OH^- exchange and (Bi) H^+-Cl^- cotransport. Schematics of six-state scheme for (Aii) Cl^-/OH^- exchange and (Bii) H^+-Cl^- cotransport and eight-state scheme for (Aiii) Cl^-/OH^- exchange and (Biii) H^+-Cl^- cotransport. The circular arrows denote direction of net transporter activity. Transition between different conformational states (s_1-s_6 or s_1-s_8) of the transporter is indicated by the straight arrows. Ion binding or unbinding to various states is indicated by the curved lines that merge with the transition arrows. The equilibrium constant for each ion binding and unbinding is represented by the parameters K_{Cl} , K_{OH} , and K_{H} for the respective ions.

($\sim 2\%$ inhibition, calculated from the modifier-site model described below). The six-state Cl^-/OH^- exchange scheme (Fig. 6 Aii) has a single extracellular/intracellular binding site, and so extracellular Cl^- and OH^- ions will compete for binding. The V_{max} for acid influx, at saturating Cl^- concentration, should thus be independent of changes of pH_o , as shown by the definition of the maximum flux (Eq. 3) derived from Appendix Eq. 18:

$$V_{\text{Max}} = \frac{[\text{H}^+]_i k_2^+ K_{\text{H}} k_1^+}{[\text{H}^+]_i k_2^+ K_{\text{H}} + [\text{H}^+]_i K_{\text{H}} k_1^+ + K_{\text{H}}^2 k_1^+}. \quad (3)$$

As the experimental value for V_{max} increased upon reduction of pH_o (Fig. 4 B), we can reject the six-state exchanger formulation of CHE. The same experimental dataset also permits the rejection of the six-state cotransporter scheme (Fig. 6 Bii). This model has four permutations, each with a dif-

ferent order of binding or unbinding of Cl^- and H^+ on the extracellular and intracellular configurations of the carrier. Depending on the permutation, the maximum H^+ -equivalent influx through CHE, with zero Cl_i^- and saturating Cl_o^- concentration (i.e., the condition immediately after readdition of 140 mM Cl_o^- shown in Fig. 4 A), is predicted to respond to changes of pH_o in a way that does not match the experimental results.

For example, two of the four permutations require H^+ to bind before Cl^- in the extracellular conformation. In these cases, in the presence of saturating levels of Cl_o^- , V_{\max} will be given by Eqs. 4 and 5 (these equations refer respectively to the situation where H^+ subsequently unbinds first or second at the intracellular site of the transporter):

$$V_{\max} = \frac{k_2^+ k_1^+}{k_2^+ + k_1^+}, \quad (4)$$

$$V_{\max} = \frac{k_2^+ K_H k_1^+}{[\text{H}^+]_i k_2^+ + [\text{H}^+]_i k_1^+ + K_H k_1^+}. \quad (5)$$

Neither Eq. 4 nor Eq. 5 contains a pH_o dependence. Our experiments, however, have shown that the apparent V_{\max} under these conditions varies with pH_o (see Fig. 4 B), thus ruling out these permutations of the model.

The other two permutations require that H^+ should bind after Cl^- in the extracellular conformation. The six-state cotransporter model then predicts that changing pH_o from 7.4 to 6.4 will result in the ratio of the apparent Cl_o^- binding affinities at both pH_o values ($K_m|_{\text{pH}_o=6.4}/K_m|_{\text{pH}_o=7.4}$) being $10^{(7.4-6.4)}$ -fold larger than the ratio of V_{\max} values at both pH_o values ($V_{\max}|_{\text{pH}_o=6.4}/V_{\max}|_{\text{pH}_o=7.4}$), i.e., effects of H_o^+ and Cl_o^- on CHE activity will appear predominantly competitive. Our experimental results fail to validate this constraint, as demonstrated by the data shown in Fig. 4 B. The experiments report that the K_m ratio is 0.75 and the V_{\max} ratio is 2, such that the affinity ratio is in fact 2.67-fold smaller than the V_{\max} ratio.

To test further the viability of the six-state cotransporter scheme, the model parameters were reduced to algebraic functions of the V_{\max} and K_m values derived from the Cl_o^- -dependence data shown in Fig. 4 B (a similar method is described in Eqs. 22 and 23). This allowed the model to be reduced to one free parameter (in our case k_1^+). k_1^+ was then varied between 10^{-4} and 10^6 ; all parameter sets within this range were found to be nonviable due to the presence of negative rate constants. Given the above algebraic and numerical evidence, we conclude that a six-state cotransporter does not provide a good description of the data.

In contrast to the nonviability of the six-state model, the eight-state model of CHE readily predicts the pH_o sensitivity of Cl_o^- -activated H^+ -equivalent influx, as shown by the curves fitted to the data in Fig. 4 B. It should be noted, however, that predictions of the exchanger model (Fig. 6 Aiii) are the same as those for the cotransporter (Fig. 6 Biii). We show in the Appendix that the effects of pH_i and pH_o on H^+ -

equivalent transport are mathematically identical for both model types. Thus, although a simple model of CHE with separate binding sites for Cl^- and H^+ equivalents successfully predicts the experimental behavior of pH_i , it cannot distinguish between H^+ and OH^- ion transport. For convenience we therefore continue to refer to CHE as a Cl^- -coupled H^+ -equivalent transporter.

Modeling the pH_i and pH_o sensitivity of H^+ -equivalent transport: electroneutral CHE

Before modeling the pH sensitivity of CHE, two points were considered.

Firstly, we considered whether changes of intracellular Cl^- concentration during our experiments may be influencing our quantification of CHE's pH-sensitivity. This is unlikely to be the case for our measurements of extracellular pH (Fig. 5 C) and extracellular Cl^- sensitivity (Fig. 4), as these were made immediately after Cl_o^- readdition, when Cl_i^- concentration would have been close to zero. In contrast, CHE's intracellular pH sensitivity was assessed experimentally from the whole timecourse of acidification of pH_i after Cl_o^- readdition (Fig. 5 B). During this period, Cl_i^- concentration must rise. To allow for the effect of this on the apparent pH_i sensitivity of CHE, one must estimate the rise. Assuming a flux-stoichiometry of one Cl^- -ion coupled with one H^+ -equivalent (as described by the eight-state model), we have approximated the increase of Cl_i^- concentration by integrating H^+ -influx over time, using a numerical procedure. This approach ignores possible contributions to Cl^- entry from other transporters such as NKCC ($\text{Na}^+\text{K}^+2\text{Cl}^-$ cotransport) (25,26), but it at least recognizes that Cl_i^- concentration will vary with pH_i . A rise of Cl_i^- has been measured previously in cardiac tissue during activation of $\text{Cl}^-/\text{HCO}_3^-$ exchange (27,28).

Secondly, the pH_i sensitivity of H^+ influx exhibits cooperativity, with a Hill coefficient for H_i^+ of > 3.0 (see Fig. 5 B, inset), suggesting an allosteric H_i^+ modifier site. This site has been modeled by a scaling factor, representing the proportion of active transporters. An individual CHE transporter is assumed to be dormant when its modifier site is titrated by intracellular H^+ ions. A rise of pH_i permits dissociation of the H^+ ions, allowing the carrier to mediate ion transport. An H^+ -binding affinity at this site of $\text{pK}_a = 7.0$, with a Hill coefficient of 4.0, provides a good description of the transporter's pH_i sensitivity.

Model parameters describing the pH_i and pH_o sensitivity of CHE were derived for the eight-state electroneutral model, using the experimental dataset shown in Fig. 5 B assuming a fixed pH_i of 7.5. The transporter flux equation (Eq. 15) can be rearranged to provide analytic definitions of V_{\max} and K_m for Cl^- -activated flux (Eqs. 22 and 23, respectively). Combining these definitions with thermodynamic constraints (Appendix Eq. 11), and including the influence of $[\text{Cl}^-]_i$ accumulation and the intracellular H^+ -modifier site, leaves a single free

parameter (in our case k_1^+) to be fit to the data. The full set of fitted model parameters for the eight-state transporter is listed in Table 1. The best fit of the model to the experimental data in the main panel of Fig. 5 B is indicated by the continuous and dashed lines. The pH_i -sensitive H^+ -equivalent influx is well represented, particularly in the pH_o range 6.4–7.4. Also reproduced by the model is the pronounced leftward shift of pH_i dependence as pH_o is reduced.

Because we did not measure Cl_i^- concentration changes directly in our experiments, but only inferred them from CHE-driven changes of pH_i , we tested whether the pK_i and H_i^+ -cooperativity values (derived by fitting the model to the experimental data) were affected by doubling the Cl^- influx assumed for each H^+ -equivalent influx. In experiments like those shown in Fig. 5 A, this would then double the predicted increase of Cl_i^- after the readdition of Cl_o^- . The output of the model was insensitive to this maneuver. There was <0.1 pH unit change in the derived value for pK_i , no change in the Hill coefficient for H_i^+ , and $<2.5\%$ change in the other transporter parameters. It therefore seems unlikely that failure to take adequate account of changes of $[\text{Cl}^-]_i$ will have significantly distorted our derivation of CHE's pH_i sensitivity.

Modeling the pH_i and pH_o sensitivity of H^+ -equivalent transport: electrogenic CHE

As well as exploring the ability of a $1\text{Cl}^-/1\text{OH}^-$ (H^+) electroneutral transporter to satisfy the Cl^- and pH dependence of CHE activity, we also investigated the predictions of an electrogenic transporter. A recent report proposes that the dominant cause of CHE activity in murine ventricular myocytes is the SLC26A6 gene product (11), which may operate with a $1\text{Cl}^-/2\text{OH}^-$ stoichiometry (12–14). An electrogenic exchanger mandates a more complex computational model, as illustrated in Fig. 7. This has a minimum of 12 states, to account for the additional binding of substrate (OH^-) to transport sites on the carrier. By assuming that the membrane potential of a ventricular cell is relatively constant after Cl_o^- readdition, the electrical driving force acting on the electrogenic carrier will also be constant (replacing Cl_o^- with an impermeant anion induces a change of membrane potential of a few mV only (23,29)). The voltage sensitivity of transport is

TABLE 1 Parameters used in simulations

Parameter	8-state electroneutral	12-state electrogenic
K_{Cl}	5.64 mM	6.12 mM
K_{H}	$10^{-4.292}$ mM	$10^{-4.558}$ mM
K_a	$10^{-4.0}$ mM	$10^{-4.0}$ mM
n_a	4.0	4.0
k_2^+	0.0165 s^{-1}	0.0158 s^{-1}
k_2^-	0.0424 s^{-1}	$3.186 \times 10^{-4} \text{ s}^{-1}$
k_1^+	1.2782 s^{-1}	2.425 s^{-1}
k_1^-	0.4983 s^{-1}	0.7856 s^{-1}

Electrogenic (Cl^- - 2H^+) and electroneutral (1Cl^- - 1H^+) CHE model parameters derived from $[\text{Cl}^-]_o$ and pH_i - pH_o kinetic data. K_a and n_a are the allosteric binding site affinity constant and Hill coefficient, respectively.

not therefore coded specifically into the model, and becomes subsumed into the model parameters (see Appendix).

As with the electroneutral model of CHE, the H^+ -equivalent flux predictions of the electrogenic CHE model can be shown to be identical for OH^- or H^+ ion transport (assuming random-order binding of Cl^- and OH^- in the cotransport model; see Appendix). For simplicity, in Fig. 7, we show only the exchanger ($1\text{Cl}^-/2\text{OH}^-$) scheme. The effect of $[\text{Cl}^-]_i$ -changes on carrier activity were again incorporated into the model by integrating H^+ -equivalent flux over time, but adjusted for the new ionic stoichiometry. The model made identical predictions as electroneutral CHE for Cl^- activation of acid influx, and its sensitivity to pH_o (*solid* and *dashed lines* through data shown in Fig. 4 B). As with the electroneutral model, the electrogenic model could be fitted reasonably well to the pH_i -dependent data shown in Fig. 5 B, with the notable exception that, contrary to experimental observation, CHE was predicted to remain essentially dormant at pH_o 8.4 (note that flux in pH_o 8.4 was not estimated at very low pH_i , as the kinetics of the $1\text{Cl}^-/2\text{OH}^-$ carrier close to its reversal pH are not readily predicted without a more formal coding for charge movement). Model parameters derived from the fitting procedure are listed in Table 1. The best fit (*shaded solid* and *dashed lines* in Fig. 5 B) required incorporation of an allosteric H_i^+ -modifier site of pK 7.0 with a Hill coefficient of 4.0 (in the model this particular Hill coefficient was constrained to be an integer number). These allosteric parameters are virtually identical to those derived for the electroneutral model. It is notable that the best-fits for electroneutral and electrogenic models to the data in Fig. 5 B are very similar in the pH_o range 6.4–7.4, predicting similar H_i^+ cooperativity values for CHE inhibition of 3–4.

Testing predictions of the eight- and twelve-state models

The electroneutral and electrogenic models were tested in three ways.

Firstly, they were used to predict the pH_o sensitivity of H^+ influx shown in Fig. 5 C (*solid line* for electroneutral, and *dashed line* for electrogenic models). Simulations were performed with initial $[\text{Cl}^-]_i = 0$ mM, $[\text{Cl}^-]_o = 140$ mM, $\text{pH}_i = 7.69$, and pH_o between 6.0 and 8.5. Results of the simulations match the experimental data (*solid circles*) reasonably well, although the electroneutral model gave the better overall fit (the L2 norm of the error is $\|e\|_2 = 0.1463$ and $\|e\|_2 = 0.2071$ for the electroneutral and electrogenic carriers, respectively). Interestingly, despite the fact that the electrogenic model comprises the transport of two OH^- ions for each Cl^- , the overall H_o^+ cooperativity predicted by the model was 1.49, much less than 2.0. This is to be compared with the predicted H_o^+ cooperativity of 1.0 for the electroneutral model.

Secondly, both models predict saturation of H^+ -equivalent influx at pH_i values higher than ~ 7.5 (Fig. 5 B). Although

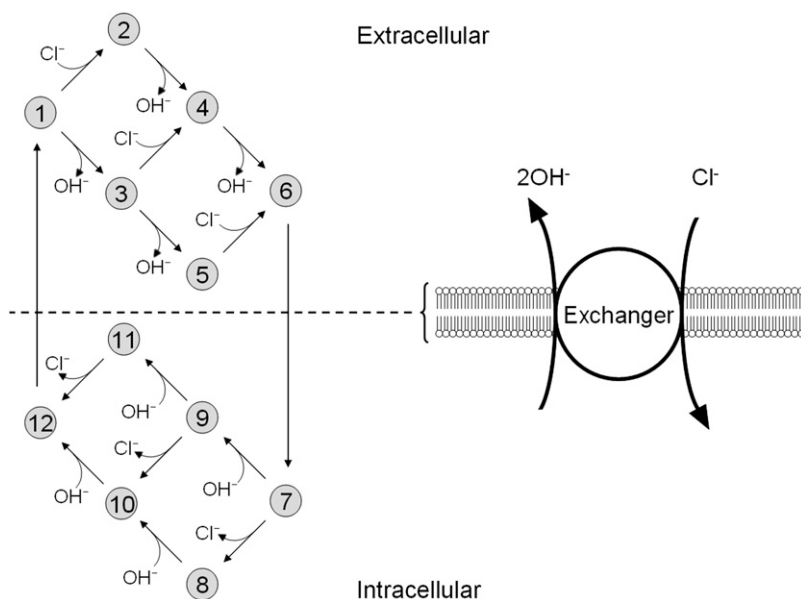


FIGURE 7 Schematic diagram for the 12-state kinetic CHE model. Twelve-state schematic diagram (*left panel*) for electrogenic $\text{Cl}^-/2\text{OH}^-$ exchange (*cartoon in right panel*, denoting net direction of transmembrane operation of transporter). The 12-state model contains three independent binding sites, two for binding OH^- ions and one for Cl^- . The binding affinities are independent of the carrier conformation and number of ions bound. The model does not distinguish between the two OH^- binding sites, which both have the same binding affinity. Transitions 1–6 occur when binding sites are exposed to the extracellular compartment. Transitions 7–12 occur when binding sites are exposed to the intracellular compartment. Transitions from consecutive odd- to even-numbered states (e.g., S1 to S2) involve Cl^- binding/unbinding. Transitions between consecutive even-numbered states (e.g., S2 to S4) or between consecutive odd-numbered states (e.g., S1 to S3) involve OH^- binding/unbinding. Rate constants and binding affinities have been omitted for clarity.

such high pH_i levels were not explored experimentally in Fig. 5 B, there was a tendency toward flux-saturation as pH_i increased (compare with data obtained at pH_o 8.4 and 7.4). High pH_i levels were, however, tested in the experiments summarized in Fig. 1 B, and clear flux-saturation at pH_i 7.6 was obtained, thus confirming the model prediction.

Thirdly, the models were tested by simulating the effect on pH_i of activating CHE, and comparing results with published experimental data from Fig. 3 of Leem and Vaughan-Jones (7) (Fig. 8 A). Fig. 8 B superimposes the timecourses of pH_i change observed in the experiment (*dashed line*) with model simulations (*continuous lines*) for electroneutral ($1\text{Cl}^-/1\text{OH}^-$) (Fig. 8 Bi) and electrogenic ($1\text{Cl}^-/2\text{OH}^-$) (Fig. 8 Bii) carriers. The experimental trace was recorded in nominally $\text{CO}_2/\text{HCO}_3^-$ -free, HEPES buffered solution, in a guinea-pig ventricular myocyte. The pH_i was initially alkalinized using an 80 mM acetate prepulse in Cl^- -free solution. Re-adding 145.5 mM Cl_o^- then activated CHE, producing a slow recovery of pH_i from the intracellular baseload. The experiment was simulated assuming that, for $\text{pH}_i > 7.1$, CHE mediates all H^+ -equivalent transport, an assumption supported by the stability of high pH_i in Cl^- -free solution (Fig. 8 A). For $\text{pH}_i < 7.1$, NHE is active, and this was simulated as a simple function of pH_i (Eq. 6), while a background H^+ flux (J_{BG}) was set to 0.025 mM s^{-1} (30). The simulated timecourses of pH_i recovery upon activating CHE are shown in Fig. 8 B, and match well the experimentally recorded timecourse.

$$J_{\text{NHE}} = -0.7852 \frac{[\text{H}^+]_i^{2.134}}{[\text{H}^+]_i^{2.134} + (10^{-3.376})^{2.134}} \text{ mM s}^{-1}. \quad (6)$$

The timecourse of pH_i change during the acetate prepulse was simulated using the approach adopted by Leem et al. (4)

and outlined below, where $\alpha = \exp(-V_m F/RT)$, $V_m = -80 \text{ mV}$, $P_{\text{HAc}} = 6.77 \times 10^{-8} \text{ cm s}^{-1}$, $P_{\text{Ac}} = 0.12 \text{ cm s}^{-1}$, $K_{\text{Ac}} = 10^{-1.528} \text{ mM}$, and $\rho = 2017 \text{ cm}^{-1}$ (7). F , R , and T are Faraday's constant, the gas constant, and temperature, respectively. Extracellular ionized and nonionized acetate concentrations were calculated using $\text{HAc}_o = \text{Ac}_{\text{tot}o}[\text{H}^+]_o / (K_{\text{Ac}} + [\text{H}^+]_o)$ and $\text{Ac}_o = \text{Ac}_{\text{tot}o} - \text{HAc}_o$, respectively:

$$J_{\text{HAc}} = \rho P_{\text{HAc}} \left(\text{HAc}_o - \frac{[\text{H}^+]_i}{[\text{H}^+]_i + K_{\text{Ac}}} \text{Ac}_{\text{tot}i} \right) \text{ mM s}^{-1},$$

$$J_{\text{Ac}} = \frac{\rho P_{\text{Ac}} V_m F}{1 - \alpha RT} \left(\text{Ac}_o - \alpha \frac{K_{\text{Ac}}}{[\text{H}^+]_i + K_{\text{Ac}}} \text{Ac}_{\text{tot}i} \right) \text{ mM s}^{-1},$$

$$\frac{d\text{Ac}_{\text{tot}i}}{dt} = J_{\text{HAc}} + J_{\text{Ac}} \text{ mM s}^{-1}. \quad (7)$$

To compute CHE-mediated H^+ -equivalent flux, it was necessary to take account of changes of $[\text{Cl}^-]_i$ during CHE activation, assuming all Cl^- flux was through CHE and either a 1:1 or 2:1 H^+ -equivalent: Cl^- stoichiometry for CHE. Changes of pH_i were modeled using Eq. 8, where β_{int} was defined in mM per pH unit based on Zaniboni et al. (20):

$$\frac{d\text{pH}_i}{dt} = -\frac{1}{\beta_{\text{int}}} \left(J_{\text{NHE}} + J_{\text{CHE}} + J_{\text{BG}} + \frac{K_{\text{Ac}}}{[\text{H}^+]_i + K_{\text{Ac}}} J_{\text{HAc}} - \frac{[\text{H}^+]_i}{[\text{H}^+]_i + K_{\text{Ac}}} J_{\text{Ac}} \right) \text{ s}^{-1}. \quad (8)$$

We conclude that the Cl^- and pH dependence of CHE does not permit one to distinguish readily between possible electroneutral and electrogenic configurations; both models predict most pH_i changes reasonably accurately. The electroneutral model, however, provides the better overall fit to the data. In particular, at high values of pH_o ($= 8.4$), the

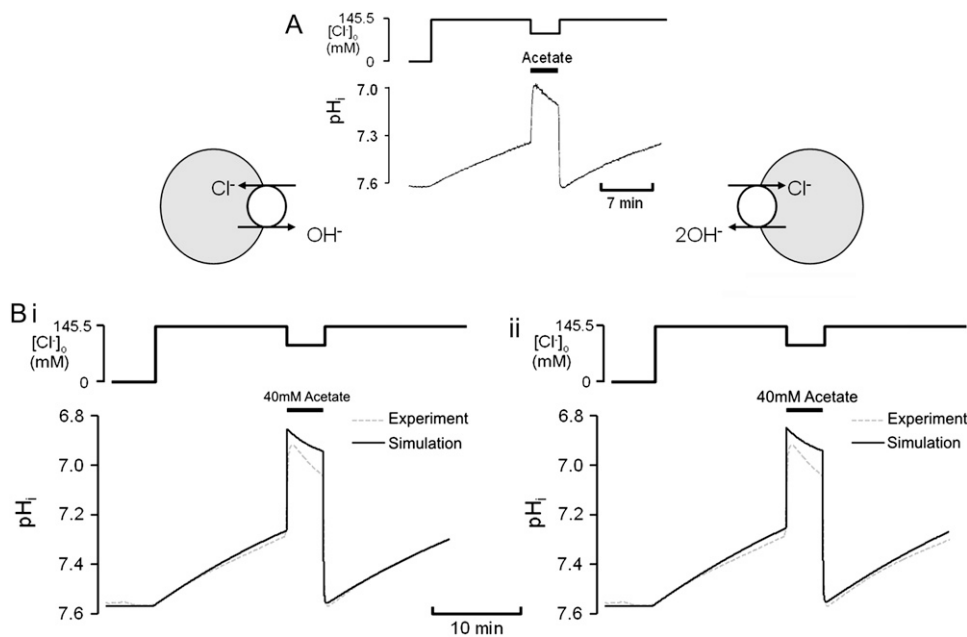


FIGURE 8 Modeling pH_i changes induced by CHE activity. (A) pH_i time-course measured experimentally, showing pH_i recovery from intracellular baseload induced first by readdition of Cl^-_o , followed by a subsequent 40 mM acetate prepulse and another pH_i recovery from the baseload (trace taken from Fig. 3 of (7)). (B) Model simulations (solid traces) of the experiment shown in panel A, based on (i) electroneutral Cl^-/OH^- exchange (eight-state model; see Fig. 6 Aiii) or (ii) electrogenic $Cl^-/2OH^-$ exchange (12-state model; see Fig. 7). The experimental timecourse has been superimposed (dashed trace in Bi and Bii).

electrogenic model predicts little or no pH_i -dependent activity, which is clearly contrary to experimental findings. Furthermore, the lack of voltage sensitivity of CHE over a wide range (-80 to $+80$ mV), although not specifically explored in the models, cannot be reconciled with an exclusive role for the electrogenic transporter.

DISCUSSION

Physiological regulation of CHE activity is by pH

In this work, we have experimentally characterized and then mathematically modeled the dependence of cardiac CHE activity on the concentrations of its transported substrates. The system conducts H^+ equivalents into the ventricular myocyte in a Cl^- and pH-dependent manner (Fig. 5, B, and C). It can do this even under stringent CO_2/HCO_3^- -free conditions, when the intracellular metabolic generation of CO_2/HCO_3^- is inhibited with cyanide or rotenone, and atmospheric CO_2 has been eliminated (Fig. 2). Acid influx via CHE cannot, therefore, result from the transport of HCO_3^- ions out of the cell. This result consolidates other reports for CHE (6,9), although a dependence of CO_2/HCO_3^- -free flux on Cl^-_o has not previously been demonstrated. We conclude that CHE involves the coupled movement of Cl^- and H^+ or OH^- ions.

The activation of CHE by different concentrations of extracellular Cl^- (Hill coefficient ~ 0.80 , Fig. 4 B) suggests a single Cl^- -ion binding site on the extracellular facing configuration of the carrier molecule. As the apparent equilibrium constant for Cl^-_o ($K_{app,Cl_o} \sim 7$ mM) is >10 -fold lower than extracellular Cl^- concentration (~ 120 mM), the Cl^- -

binding site will normally be close to saturation. Natural variation of plasma $[Cl^-]_o$, which can be in the range ± 5 – 10 mM (e.g., (31)), will not significantly change CHE activity, suggesting the transporter is not a physiological sensor of $[Cl^-]_o$. In contrast, CHE activity varies greatly with changes of pH_i and pH_o in the physiological range (see Fig. 5, B and C). Thus, CHE will serve as a physiological pH sensor, its activity being tightly regulated by pH on either side of the sarcolemma.

Despite two different possible modes of H^+ -equivalent transport via CHE (utilizing either OH^- or H^+ ions), CHE functions, in pH terms, like a proton-gated leak of hydrochloric acid into the cell, as illustrated schematically in Fig. 9 A. The leak is stimulated by extracellular H^+ ions, but inhibited by intracellular H^+ ions. It is likely to contribute to the dependence of steady-state pH_i on pH_o in the cardiac cell. On average, resting pH_i in ventricular myocytes falls by nearly 40% of a tonic fall in pH_o , and much of the acid influx that underpins this is conducted via CHE (6). In the short term, the influx may help to buffer an extracellular acidosis, by transferring the acid onto intracellular buffer sites. The magnitude of the accompanying decline of pH_i will eventually be limited by the inhibitory effect of intracellular H^+ ions on acid influx, and also by acid extrusion on transporters such as NHE and NBC, which are themselves regulated by pH_i and pH_o (for review, see (32)). In the presence of CO_2/HCO_3^- buffer, the acid-influx role of CHE will be supplemented by HCO_3^- efflux on the cardiac Cl^-/HCO_3^- exchanger (7). Thus cardiac CHE appears to be specialized as part of a multi-transporter complex that controls pH_i . In epithelial tissues, CHE has been proposed, variously, to be a controller of either pH_i (rat distal colon; (33)) or Cl^-_i (rat duodenal brush border

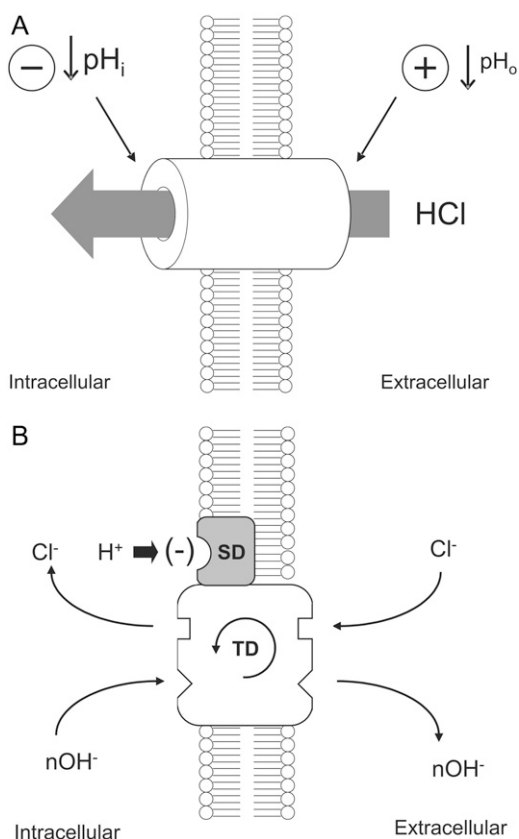


FIGURE 9 Schematic diagrams of CHE. (A) CHE acts, in effect, as a leak of hydrochloric acid into the cardiac cell, regulated by pH_i (low pH inhibitory) and pH_o (low pH excitatory). (B) CHE represented as Cl^-/OH^- exchange, showing separate transport binding sites for intracellular and extracellular Cl^- and OH^- ($n = 1,2$) ions, positioned on the transport domain (TD) of the carrier. Ion transport is also regulated by a proton-binding, allosteric controller (the proton sensor domain, SD) positioned on the intracellular face of the protein. Proton binding to the SD inhibits carrier activity.

membrane; (34)). In the latter case, Cl_o^- affinity appears much lower than for cardiac CHE, as might be expected for a physiological sensor of extracellular Cl^- concentration (16).

H^+-Cl^- cotransport versus Cl^-/OH^- exchange

Our modeling of CHE indicates that Cl^-/OH^- exchange and H^+-Cl^- cotransport modes of activity would display the same kinetic behavior, with respect to membrane fluxes of Cl^- and intracellular changes of pH. This is because the general form of the eight-state or twelve-state exchange and random-order binding cotransport models means they are mathematically equivalent. They cannot therefore be distinguished using flux data alone. A previous analysis of epithelial CHE (16) suggested H^+-Cl^- cotransport is the more likely configuration. In that report, exchangers were assumed to be unable to form ternary complexes, i.e., they bind only one of the two transported substrates at any moment. For

electroneutral Cl^-/OH^- exchange this meant, in effect, that Cl^- and OH^- ions compete for binding to a single site on the carrier. This led to the adoption of a six-state model for the exchanger-mode of CHE, while a minimum description of electroneutral H^+-Cl^- cotransport required an eight-state model (with separate sites for simultaneous H^+ and Cl^- ion binding). Such models can, in theory, be distinguished kinetically. The exchanger will show competition between transported substrates while the cotransporter will not. Both epithelial and cardiac CHE display a predominantly non-competitive interaction between H_o^+ equivalents and Cl_o^- , which might be taken to indicate H^+-Cl^- cotransport, as proposed by Alvarado and Vasseur (16). There is no compelling reason, however, to assume that all exchangers are nonternary. Furthermore, other putative exchangers, like Na^+/H^+ exchange, display competitive (24), noncompetitive (35), or mixed (36) substrate interactions, a reflection possibly of the different NHE isoforms dominant in different tissues. While exchangers are likely to obey ping-pong kinetics for the transport step, with only one type of substrate moving at any moment across the membrane, this does not preclude the possibility of ternary complexes forming reversibly on the external or internal facing configuration of the carrier, as illustrated for the eight-state (electroneutral) and twelve-state (electrogenic) models shown in this work (e.g., Fig. 6 Aiii and Fig. 7). In these cases the predicted kinetic behavior of the exchanger model does not differ from the similar-state cotransporter model. A distinction between H^+ and OH^- modes of transport cannot therefore be made. For convenience, however, we continue to use the acronym "CHE" when referring to the cardiac transporter, while recognizing that the mode of transport has yet to be resolved.

Conformation-dependent substrate binding affinities?

One assumption in our modeling is that the substrate binding affinities of cardiac CHE are constant throughout different stages of the transport cycle. We made this simplifying assumption as there is no evidence, as yet, to the contrary. Nevertheless, asymmetry in substrate binding affinity has been detected experimentally for extracellular and intracellular facing configurations of the AE1 Cl^-/HCO_3^- exchanger (37), and for other more complex carriers such as the Na^+/K^+ ATPase (see (38)). We do not exclude a similar asymmetry for CHE, despite the fact that the carrier is probably not a protein product of the AE gene family. We can only infer the real binding affinities for H^+ , OH^- , or Cl^- from our present measurements of apparent binding affinities, taken when the full transport cycle for CHE has been activated. More sophisticated experiments on partial reactions within the cycle will be needed to probe any sidedness of real affinity. We have, however, been able to exclude the possibility that the presence of asymmetry defines the minimum number of transition states (six or eight) required for modeling either

Cl^-/OH^- or H^+-Cl^- modes of electroneutral transport. When assuming asymmetric extracellular and intracellular substrate affinities, a minimum of eight states is still required for both modes, reinforcing the conclusion that they cannot be distinguished kinetically.

The gene product for CHE: electroneutral versus electrogenic transporters

Armed with the transport properties of cardiac CHE, one may ask which gene product underlies the process. Insensitivity of the carrier to high concentrations of DIDS (0.5 mM) (6,7) and to $\text{CO}_2/\text{HCO}_3^-$ removal (7,9) suggests that it is not a known member of the AE (SLC4A) family of bicarbonate transporters. This conclusion is further supported by recent evidence that SLC4A3 and SLC4A1 in heterologous expression systems appear to support $\text{Cl}^-/\text{HCO}_3^-$ but not Cl^-/OH^- exchange (11,39); however, counter-results have been reported (13). Casey and co-workers (11) suggest that CHE in guinea-pig heart may, instead, be an SLC26A6 gene product, particularly as the relevant mRNA and protein products are heavily expressed in murine ventricular tissue. While some studies have suggested that the SLC26A6 protein does not support Cl^-/OH^- exchange (40,41), others have concluded that it does (12–15). SLC26A6 transfected into HEK293 cells results in the functional appearance of Cl^-/OH^- exchange, as judged from Cl_0^- -dependent changes of pH_i in $\text{CO}_2/\text{HCO}_3^-$ -free conditions (11). The changes, however, are inhibited by high concentrations of DIDS, as expected for SLC26A6 gene products, and they are enhanced in the presence of $\text{CO}_2/\text{HCO}_3^-$ buffer, suggesting HCO_3^- ions are also transported on the carrier, two features that are not evident for cardiac CHE (6,7).

One property of the SLC26A6 anion exchanger that has attracted particular attention recently is its possible electrogenic activity. Evidence for the transport stoichiometry is contentious, with reports for both 2OH^- (or HCO_3^-)/ 1Cl^- electrogenic (12–14) and 1OH^- (or HCO_3^-)/ 1Cl^- electroneutral activity ((15). Heterologous expression of SLC26A6 results in a voltage-sensitive membrane current (13,14), proposed to reflect electrogenic OH^- (or HCO_3^-) transfer through the carrier, although some (15) have suggested the current may not be linked directly to transport stoichiometry. It is notable that H^+ -equivalent influx through cardiac CHE is insensitive to large excursions of membrane potential from +80 to –80 mV, consistent with a previous report employing smaller voltage jumps of ± 40 mV (6). Such voltage insensitivity can be reconciled with an electroneutral (Fig. 6) but not an electrogenic transporter (Fig. 7). The voltage range tested should have terminated or even reversed H^+ -equivalent flux through a 2OH^- (or HCO_3^-)/ 1Cl^- exchanger, thus excluding it as the sole component of cardiac CHE.

We investigated whether the pH_i and pH_o dependence of CHE may provide a clue to the carrier's underlying stoichiometry. The movement of two OH^- ions per electrogenic

carrier cycle (Fig. 7) could conceivably result in a higher level of H_i^+ and H_o^+ cooperativity for flux activity than for a simple electroneutral carrier (Fig. 6) that exchanged only one OH^- ion per cycle. Our computational modeling, however, indicates that using substrate dependence to distinguish transport-stoichiometry may not be straightforward. The models show that the steep H_i^+ cooperativity measured experimentally for cardiac CHE may be dominated by H^+ binding to an allosteric modifier site, and little affected by transport stoichiometry. Furthermore, H_o^+ cooperativity, which should be determined largely by extracellular OH^- unbinding from the carrier, is predicted in the models to vary from 1.0 for an electroneutral carrier to just under 1.5 for the electrogenic carrier. Such modest differences in cooperativity may be difficult to measure experimentally with a high degree of confidence. Nevertheless, an H_o^+ cooperativity of 0.96 was measured experimentally in this work, which would tend to support the electroneutral configuration. The cooperativity of activation of CHE by Cl_0^- provides no additional clue as, for both types of carrier, it should equal 1.0, given that only one Cl^- ion per cycle participates in each scheme. Indeed, experimentally measured Cl_0^- cooperativity was in this range (0.76–0.86, Fig. 4 B).

The evidence that SLC26A6 underpins CHE activity in heart is therefore equivocal. If one argues that the SLC26A6 carrier is electrogenic with a $1\text{Cl}^-/2\text{OH}^-$ (or HCO_3^-) stoichiometry, then it should display clear voltage sensitivity, and this has not been observed for CHE in guinea-pig myocytes (Fig. 3). This could indicate either that the SLC26A6 carrier in heart is electroneutral, or that voltage sensitivity is disguised by the presence of another H^+ -equivalent transporter. It is of interest, therefore, that SLC26A3 gene products have been detected in murine ventricular tissue (11), in addition to SLC26A6. The protein product appears to support $\text{Cl}^-/\text{HCO}_3^-$ and Cl^-/OH^- exchange when expressed heterologously in *Xenopus* oocytes and HEK293 cells (11,13,14), but it is suggested to operate with an opposite transport stoichiometry to that of electrogenic SLC26A6, exchanging 1OH^- (or HCO_3^-) ion for two or more Cl^- ions (13,14). This carrier cannot, by itself, account for H^+ -equivalent influx through cardiac CHE as, under resting physiological conditions (membrane potential at ~ -80 mV), it would be energized thermodynamically to promote H^+ -equivalent efflux (at pH_i 7.2, E_{CHE} would be -50 mV, see Fig. 3 B). Furthermore, there is no evidence for Cl^- -sensitive acid efflux from the mammalian ventricular myocyte (17). But a $2\text{Cl}^-/1\text{OH}^-$ transporter should be voltage-sensitive and, during depolarization of the membrane potential positive to the transporter's equilibrium potential, it may reverse (see Fig. 3 B) to provide H^+ -equivalent influx. Thus, while H^+ -equivalent influx through electrogenic SLC26A6 may decrease with depolarization, influx through SLC26A3 may conceivably increase.

As pointed out by Ko et al. (13), coexpression of electrogenic SLC26A6 and SLC26A3 gene products in the same

cell membrane could result in a functionally electroneutral Cl^-/OH^- (HCO_3^-) system that still mediated a net acid flux. For this to happen in a ventricular cell membrane, the kinetic activity and expression levels of the two opposing H^+ -equivalent carriers would need to be finely balanced so as to eliminate any voltage sensitivity of H^+ -equivalent flux. Such a balance would be remarkably fortuitous, unless coexpression and functional activity of the transporters were mechanistically coordinated in some way. Expression of the transporters was not measured in the guinea-pig ventricular myocytes used in this work. Indeed, protein expression has so far only been reported for SLC26A6 in murine ventricular myocytes (11). Nevertheless, in the latter cells, mRNA transcripts for both transporters were readily detected, but SLC26A6 expression was 100-fold greater than for SLC26A3. If sarcolemmal protein expression were to match transcript levels, it would be difficult to see how opposing flux activity in the two transporters could be balanced so precisely, particularly during rapid jumps of membrane potential. Differences, however, in transporter expression between guinea-pig and mouse cannot be excluded, especially as the functional expression of other H^+ -equivalent transporters, such as $\text{Na}^+/\text{HCO}_3^-$ cotransport, can vary dramatically among species (22). The question of the identity of the transporters contributing to cardiac CHE activity must therefore remain open. What can be concluded is that CHE flux conforms well to an electroneutral Cl^-/OH^- exchanger, controlled by pH_i and pH_o , and this excludes sole contribution from an electrogenic SLC26A6 transporter. Given that H^+/Cl^- and Cl^-/OH^- modes of transport cannot be distinguished kinetically, the possibility must also remain that cardiac CHE in guinea-pig myocytes is mediated via a novel H^+/Cl^- cotransport protein.

Proton sensor domain

The steep dependence of cardiac CHE activity on pH_i (Fig. 1 and Fig. 5 B) is in contrast to the previous linear dependence reported by Leem et al. (4). This difference can be attributed to higher resolution measurements in this work, performed over a broader range of pH_i values. Our computational modeling suggests that, irrespective of whether electroneutral (i.e., 1OH^-) or electrogenic (i.e., 2OH^-) transport is assumed, the high H_i^+ cooperativity measured experimentally for CHE cannot be simulated unless an intracellular modifier site for H^+ (or OH^-) ions is introduced, of $\text{pK} \sim 7.0$ and Hill coefficient 4.0. Thus the transporter may possess two functional domains. One domain, accessed from both the internal and external environment, would mediate substrate binding and transport. Given that one of the substrates is an H^+ -equivalent ion, this would immediately confer some pH sensitivity on the system. For example, extracellular H^+ -binding to the transport domain (TD) is the main explanation in our models for the pH_o sensitivity of CHE (Fig. 5 C). The other domain, accessed from only the internal environment, would mediate H^+ -equivalent sensing

and subsequent modulation of transporter flux. H^+ -binding to this sensor domain (SD) in the CHE model accounts for most of the steep inhibitory effect of low pH_i on CHE activity. TD and SD regions on the carrier are illustrated schematically for Cl^-/OH^- exchange mode in Fig. 9 B.

We chose to model the SD by assuming that an individual carrier molecule is inactive until its intracellular SD region is occupied by four OH^- ions (or, equivalently, when four H^+ ions unbind from the domain). This will occur when pH_i rises from its resting value. Such a model would not preclude the siting of SD within a multimeric rather than a monomeric carrier protein. The concept of distinct SD and TD regions for a carrier has previously been proposed to account for high H_i^+ cooperativity in the activation of NHE (24,35,42–44). An alternative NHE model involves oscillating dimers whose subunits have radically different H_i^+ affinities (45). This latter model was not pursued in this work, because it is limited to H_i^+ cooperativity values between 1.0 and 2.0—lower than the level of cooperativity observed for CHE.

A low rather than a high cooperative effect of H_i^+ has been reported for enterocyte apical brush-border membrane CHE (16), where the Hill coefficient for H_i^+ binding is 0.46. This low value was suggested to be caused by slippage of H^+ transport through the carrier. The apparent difference in pH_i sensitivity of cardiac and epithelial CHE is dramatic and may reflect the expression of different H^+ -equivalent transport molecules in the two tissues. The difference may also reflect different physiological functions for the two types of transporter, with the greater emphasis on pH_i regulation for cardiac CHE. It is notable, however, that direct pH_i measurements in intact cells were not made when estimating H_i^+ cooperativity of epithelial CHE (16). Instead, experiments were performed on BBM vesicles, where values for intravesicular pH were assumed. The possibility of errors in the estimate of epithelial CHE's pH_i sensitivity should not therefore be excluded.

CONCLUSIONS

The transport properties of cardiac CHE are consistent with either Cl^-/OH^- exchange or H^+/Cl^- cotransport. The flux activity of CHE can be best fit by an electroneutral, voltage-insensitive mechanism, whose activity is tightly regulated by pH_i and pH_o . Whether CHE reflects a single type of transporter or a precisely coordinated combination of different transporters remains to be resolved. In effect, the CHE system acts like an H^+ -gated leak of HCl into the cell (Fig. 9 A). This leak will be particularly important in the regulation of cardiac pH_i , not only during acute displacements of extracellular pH, but also during displacements of pH_i from its steady state. When pH_i is close to its resting value, the magnitude of CHE-mediated acid influx in the intact myocyte (Figs. 1 B and 5 B) is comparable to that through the cell's other acid-loading transporter, $\text{Cl}^-/\text{HCO}_3^-$ exchange, and comparable to H^+ -equivalent extrusion through Na^+/H^+

exchange and $\text{Na}^+\text{-HCO}_3^-$ cotransport (4). H^+ -dependent regulation of CHE is thus an important component of the system that sets resting pH_i , and hence basal function in the heart.

APPENDIX

Electroneutral carrier models

Here we provide a detailed derivation of the eight-state, electroneutral, independent-binding cotransporter model (Fig. 6 Biii). The remaining three electroneutral models can be derived by applying the same principles over analogous steps.

At equilibrium, the rates of transition between consecutive states in the transport cycle must be equal, resulting in the set of relations described by

$$\begin{aligned} S_1 \frac{[\text{Cl}^-]_o}{K_{\text{Cl}_o}} &= S_3 & S_2 &= S_1 \frac{[\text{H}^+]_o}{K_{\text{H}_o}} \\ S_3 \frac{[\text{H}^+]_o}{K_{\text{H}_o}} &= S_4 & S_4 &= S_2 \frac{[\text{Cl}^-]_o}{K_{\text{Cl}_o}} \\ S_4 k_2^+ &= S_5 k_2^- \\ S_5 &= S_6 \frac{[\text{H}^+]_i}{K_{\text{H}_i}} & S_7 &= S_5 \frac{[\text{Cl}^-]_i}{K_{\text{Cl}_i}} \\ S_6 &= S_8 \frac{[\text{Cl}^-]_i}{K_{\text{Cl}_i}} & S_8 &= S_6 \frac{[\text{H}^+]_i}{K_{\text{H}_i}} \\ S_8 k_1^+ &= S_1 k_1^- \end{aligned} \quad (9)$$

K_{Ax} is the dissociation constant of ion A in compartment x (i = intracellular, o = extracellular). The value S_j is the j^{th} state and k_j^+ and k_j^- are the transition rates between the extracellular and intracellular space, in which the plus (+) and minus (−) symbols correspond to the clockwise and anticlockwise directions, respectively, and where j is equal to one or two when the carrier is moving Cl^- out of or into the cell, respectively. The eight-state cotransporter contains four possible loops, resulting in the same thermodynamic constraint. For example, the product of the left- and right-hand side steady-state equations (see Eq. 9) for the loop S_1, S_3, S_4, S_5, S_7 , and S_8 are equal, resulting in

$$\frac{[\text{H}^+]_o K_{\text{H}_i} [\text{Cl}^-]_o K_{\text{Cl}_i} k_1^+ k_2^+}{[\text{H}^+]_i K_{\text{H}_o} [\text{Cl}^-]_i K_{\text{Cl}_o} k_1^- k_2^-} = 1. \quad (10)$$

Assuming that the dissociation constants are the same for both intracellular and extracellular states, and considering balanced intracellular and extracellular ion concentrations, then the thermodynamically consistent constraint is attained:

$$k_1^+ k_2^+ = k_1^- k_2^-. \quad (11)$$

Using the rapid flux transport assumption to reduce the model to two states, representing the intracellular (S_i) and extracellular (S_o) conformations, leads to

$$\begin{aligned} S_i &= S_1 \left(1 + \frac{[\text{H}^+]_o}{K_{\text{H}}} + \frac{[\text{Cl}^-]_o}{K_{\text{Cl}}} + \frac{[\text{Cl}^-]_o [\text{H}^+]_o}{K_{\text{Cl}} K_{\text{H}}} \right) \\ &= S_4 \left(1 + \frac{K_{\text{H}}}{[\text{H}^+]_o} + \frac{K_{\text{Cl}}}{[\text{Cl}^-]_o} + \frac{K_{\text{Cl}} K_{\text{H}}}{[\text{Cl}^-]_o [\text{H}^+]_o} \right), \end{aligned}$$

$$\begin{aligned} S_o &= S_8 \left(1 + \frac{[\text{H}^+]_i}{K_{\text{H}}} + \frac{[\text{Cl}^-]_i}{K_{\text{Cl}}} + \frac{[\text{Cl}^-]_i [\text{H}^+]_i}{K_{\text{Cl}} K_{\text{H}}} \right) \\ &= S_5 \left(1 + \frac{K_{\text{H}}}{[\text{H}^+]_i} + \frac{K_{\text{Cl}}}{[\text{Cl}^-]_i} + \frac{K_{\text{Cl}} K_{\text{H}}}{[\text{Cl}^-]_i [\text{H}^+]_i} \right). \end{aligned} \quad (12)$$

The rate of transition between the two states can then be described by combining Eqs. 9 and 12 to define the rates $\alpha_{1,2}^+$ and $\alpha_{1,2}^-$ in the anticlockwise and clockwise directions, respectively:

$$\begin{aligned} \alpha_1^+([\text{H}^+]_i, [\text{Cl}^-]_i) &= \frac{k_1^+}{\left(\frac{[\text{H}^+]_i}{K_{\text{H}}} + 1 \right) \left(\frac{[\text{Cl}^-]_i}{K_{\text{Cl}}} + 1 \right)}, \\ \alpha_1^-([\text{H}^+]_o, [\text{Cl}^-]_o) &= \frac{k_1^-}{\left(\frac{[\text{H}^+]_o}{K_{\text{H}}} + 1 \right) \left(\frac{[\text{Cl}^-]_o}{K_{\text{Cl}}} + 1 \right)}, \\ \alpha_2^+([\text{H}^+]_o, [\text{Cl}^-]_o) &= \frac{k_2^+ \left(\frac{[\text{H}^+]_o}{K_{\text{H}}} \frac{[\text{Cl}^-]_o}{K_{\text{Cl}}} \right)}{\left(\frac{[\text{H}^+]_o}{K_{\text{H}}} + 1 \right) \left(\frac{[\text{Cl}^-]_o}{K_{\text{Cl}}} + 1 \right)}, \\ \alpha_2^-([\text{H}^+]_i, [\text{Cl}^-]_i) &= \frac{k_2^- \left(\frac{[\text{H}^+]_i}{K_{\text{H}}} \frac{[\text{Cl}^-]_i}{K_{\text{Cl}}} \right)}{\left(\frac{[\text{H}^+]_i}{K_{\text{H}}} + 1 \right) \left(\frac{[\text{Cl}^-]_i}{K_{\text{Cl}}} + 1 \right)}. \end{aligned} \quad (13)$$

At steady state,

$$S_o = 1 - S_i = \frac{\alpha_1^+ + \alpha_2^-}{\alpha_1^+ + \alpha_2^- + \alpha_2^+ + \alpha_1^-}, \quad (14)$$

resulting in a steady-state flux of

$$J_{\text{CHE}} = \frac{\alpha_1^+ \alpha_2^+ + \alpha_2^- \alpha_1^-}{\alpha_1^+ + \alpha_2^- + \alpha_2^+ + \alpha_1^-}. \quad (15)$$

Allosteric inhibition is characterized by the addition of a Hill scaling factor, such that the flux with allosteric effects is

$$J_{\text{CHE}} = \frac{K_a^{\text{na}}}{[\text{H}^+]_i^{\text{na}} + K_a^{\text{na}}} \frac{\alpha_1^+ \alpha_2^+ + \alpha_2^- \alpha_1^-}{\alpha_1^+ + \alpha_2^- + \alpha_2^+ + \alpha_1^-}. \quad (16)$$

This allosteric mechanism assumes that when an H^+ sensor site, with a binding affinity of K_a and cooperativity of na , is occupied by H^+ ions, the transporter is unable to function.

With each of the four models proposed, the transporter is described by Eq. 16 with the definition of the α -values changing with each model. The definition of α for the six-state (with $[\text{Cl}^-]_o\text{-}[\text{H}^+]_o$ binding and $[\text{H}^+]_i\text{-}[\text{Cl}^-]_i$ unbinding order) state cotransporter and the six- and eight-state exchangers are defined in Eqs. 17–19, respectively. The six-state cotransporter (see Fig. 6 Bii) α -values are

$$\begin{aligned} \alpha_1^+([\text{H}^+]_i, [\text{Cl}^-]_i) &= \frac{k_1^+}{\left(1 + \frac{[\text{H}^+]_i}{K_{\text{H}}} + \frac{[\text{Cl}^-]_i}{K_{\text{Cl}}} + \frac{[\text{H}^+]_i [\text{Cl}^-]_i}{K_{\text{H}} K_{\text{Cl}}} \right)}, \\ \alpha_1^-([\text{H}^+]_o, [\text{Cl}^-]_o) &= \frac{k_1^-}{\left(1 + \frac{[\text{H}^+]_o}{K_{\text{H}}} + \frac{[\text{Cl}^-]_o}{K_{\text{Cl}}} + \frac{[\text{Cl}^-]_o [\text{H}^+]_o}{K_{\text{Cl}} K_{\text{H}}} \right)}, \end{aligned}$$

$$\alpha_2^+([H^+]_o, [Cl^-]_o) = \frac{k_2^+ \left(\frac{[H^+]_o [Cl^-]_o}{K_H K_{Cl}} \right)}{\left(1 + \frac{[H^+]_o}{K_H} + \frac{[Cl^-]_o}{K_{Cl}} + \frac{[H^+]_o [Cl^-]_o}{K_H K_{Cl}} \right)},$$

$$\alpha_2^-([H^+]_i, [Cl^-]_i) = \frac{k_2^- \left(\frac{[H^+]_i [Cl^-]_i}{K_H K_{Cl}} \right)}{\left(1 + \frac{[H^+]_i}{K_H} + \frac{[Cl^-]_i}{K_{Cl}} + \frac{[H^+]_i [Cl^-]_i}{K_H K_{Cl}} \right)}. \quad (17)$$

The six-state exchanger (see Fig. 6 Aii) α -values are

$$\alpha_1^+([OH^-]_i, [Cl^-]_i) = \frac{k_1^+ \frac{[OH^-]_i}{K_{OH}}}{\left(1 + \frac{[OH^-]_i}{K_{OH}} + \frac{[Cl^-]_i}{K_{Cl}} \right)},$$

$$\alpha_1^-([OH^-]_o, [Cl^-]_o) = \frac{k_1^- \frac{[OH^-]_o}{K_{OH}}}{\left(1 + \frac{[OH^-]_o}{K_{OH}} + \frac{[Cl^-]_o}{K_{Cl}} \right)},$$

$$\alpha_2^+([OH^-]_o, [Cl^-]_o) = \frac{k_2^+ \left(\frac{[Cl^-]_o}{K_{Cl}} \right)}{\left(1 + \frac{[OH^-]_o}{K_{OH}} + \frac{[Cl^-]_o}{K_{Cl}} \right)},$$

$$\alpha_2^-([OH^-]_i, [Cl^-]_i) = \frac{k_2^- \left(\frac{[Cl^-]_i}{K_{Cl}} \right)}{\left(1 + \frac{[OH^-]_i}{K_{OH}} + \frac{[Cl^-]_i}{K_{Cl}} \right)}. \quad (18)$$

The eight-state exchanger (see Fig. 6 Aiii) α -values are

$$\alpha_1^+([OH^-]_i, [Cl^-]_i) = \frac{k_1^+ \frac{[OH^-]_i}{K_{OH}}}{\left(1 + \frac{[OH^-]_i}{K_{OH}} \right) \left(1 + \frac{[Cl^-]_i}{K_{Cl}} \right)},$$

$$\alpha_1^-([OH^-]_o, [Cl^-]_o) = \frac{k_1^- \frac{[OH^-]_o}{K_{OH}}}{\left(1 + \frac{[OH^-]_o}{K_{OH}} \right) \left(1 + \frac{[Cl^-]_o}{K_{Cl}} \right)},$$

$$\alpha_2^+([OH^-]_o, [Cl^-]_o) = \frac{k_2^+ \left(\frac{[Cl^-]_o}{K_{Cl}} \right)}{\left(1 + \frac{[OH^-]_o}{K_{OH}} \right) \left(1 + \frac{[Cl^-]_o}{K_{Cl}} \right)},$$

$$\alpha_2^-([OH^-]_i, [Cl^-]_i) = \frac{k_2^- \left(\frac{[Cl^-]_i}{K_{Cl}} \right)}{\left(1 + \frac{[OH^-]_i}{K_{OH}} \right) \left(1 + \frac{[Cl^-]_i}{K_{Cl}} \right)}. \quad (19)$$

The eight-state exchanger and the eight-state cotransporter are mathematically identical; this can be shown by making the substitution $[OH^-]/K_{OH} = K_H/[H^+]$ into Eq. 19, which is then equal to Eq. 13.

Electrogenic carrier models

In electrogenic models, two OH^- ions are exchanged for one Cl^- (see Fig. 8), or two H^+ ions are cotransported with one Cl^- ion across the membrane. As these carriers are electrogenic, the flux through the carrier will be voltage-dependent. Voltage dependence of cyclical carrier models can be represented by including a voltage-dependent model parameter (46). As the voltage changes experienced during experiments are likely to be nominal, we assumed that any voltage-dependent model parameter will remain constant. Because of this, we were able to simplify the model by removing voltage from the thermodynamic constraints of the system. This is energetically valid, provided $E_{CHE} > V_m$, as will have been the case for the simulations shown in this work. Inclusion of voltage in the thermodynamics of the model will, however, be required if it is to be extended to a more general case. The electrogenic model equations were derived using the same method as for the electroneutral models, ignoring any charge movement. The α -values for the 12-state exchanger are given in

$$\alpha_1^+([H^+]_i, [Cl^-]_i) = \frac{k_1^+ \left(\frac{K_H}{[H^+]_i} \right)^2}{\left(1 + \frac{K_H}{[H^+]_i} + \left(\frac{K_H}{[H^+]_i} \right)^2 \right) \left(1 + \frac{[Cl^-]_i}{K_{Cl}} \right)},$$

$$\alpha_2^+([H^+]_o, [Cl^-]_o) = \frac{k_2^+ \left(\frac{[Cl^-]_o}{K_{Cl}} \right)}{\left(1 + \frac{K_H}{[H^+]_o} + \left(\frac{K_H}{[H^+]_o} \right)^2 \right) \left(1 + \frac{[Cl^-]_o}{K_{Cl}} \right)},$$

$$\alpha_1^-([H^+]_o, [Cl^-]_o) = \frac{k_1^- \left(\frac{K_H}{[H^+]_o} \right)^2}{\left(1 + \frac{K_H}{[H^+]_o} + \left(\frac{K_H}{[H^+]_o} \right)^2 \right) \left(1 + \frac{[Cl^-]_o}{K_{Cl}} \right)},$$

$$\alpha_2^-([H^+]_i, [Cl^-]_i) = \frac{k_2^- \left(\frac{[Cl^-]_i}{K_{Cl}} \right)}{\left(1 + \frac{K_H}{[H^+]_i} + \left(\frac{K_H}{[H^+]_i} \right)^2 \right) \left(1 + \frac{[Cl^-]_i}{K_{Cl}} \right)}. \quad (20)$$

The 12-state cotransporter α -values are

$$\alpha_1^+([OH^-]_i, [Cl^-]_i) = \frac{k_1^+ \left(\frac{[OH^-]_i}{K_{OH}} \right)^2}{\left(1 + \frac{[OH^-]_i}{K_{OH}} + \left(\frac{[OH^-]_i}{K_{OH}} \right)^2 \right) \left(1 + \frac{[Cl^-]_i}{K_{Cl}} \right)},$$

$$\begin{aligned}
& \alpha_1^- ([\text{OH}^-]_o, [\text{Cl}^-]_o) \\
&= \frac{k_1^- \left(\frac{[\text{OH}^-]_o}{K_{\text{OH}}} \right)^2}{\left(1 + \frac{[\text{OH}^-]_o}{K_{\text{OH}}} + \left(\frac{[\text{OH}^-]_o}{K_{\text{OH}}} \right)^2 \right) \left(1 + \frac{[\text{Cl}^-]_o}{K_{\text{Cl}}} \right)}, \\
& \alpha_2^+ ([\text{OH}^-]_o, [\text{Cl}^-]_o) \\
&= \frac{k_2^+ \left(\frac{[\text{Cl}^-]_o}{K_{\text{Cl}}} \right)}{\left(1 + \frac{[\text{OH}^-]_o}{K_{\text{OH}}} + \left(\frac{[\text{OH}^-]_o}{K_{\text{OH}}} \right)^2 \right) \left(1 + \frac{[\text{Cl}^-]_o}{K_{\text{Cl}}} \right)}, \\
& \alpha_2^- ([\text{OH}^-]_i, [\text{Cl}^-]_i) \\
&= \frac{k_2^- \left(\frac{[\text{Cl}^-]_i}{K_{\text{Cl}}} \right)}{\left(1 + \frac{[\text{OH}^-]_i}{K_{\text{OH}}} + \left(\frac{[\text{OH}^-]_i}{K_{\text{OH}}} \right)^2 \right) \left(1 + \frac{[\text{Cl}^-]_i}{K_{\text{Cl}}} \right)}. \quad (21)
\end{aligned}$$

Fitting the model

The eight-state model parameters were fitted in three phases. First, the Hill equations, with the Hill coefficient rounded to one, were fit to the two $[\text{Cl}^-]_o$ dependent data sets, recorded at two pH_o values (see Fig. 4 B). The eight-state model equations were then manipulated to give algebraic definitions of V_{max} (Eq. 23) and K_m (Eq. 22). Rearranging these equations, and using the thermodynamic consistency equation (Eq. 11), gave algebraic definitions of K_H , K_{Cl} , k_2^+ , k_2^- , and k_1^- . In the third phase, the sole remaining parameter k_1^+ was fit to the pH_i/pH_o -dependent data (see Fig 5). This method allows us to calculate a unique parameter set for the model:

$$K_m = K_{\text{Cl}} \frac{k_1^+ \left(1 + \frac{[\text{H}^+]_o}{K_H} \right) + k_1^- \left(1 + \frac{[\text{H}^+]_i}{K_H} \right)}{k_2^+ \frac{[\text{H}^+]_o}{K_H} \left(1 + \frac{[\text{H}^+]_i}{K_H} \right) + k_1^+ \left(1 + \frac{[\text{H}^+]_o}{K_H} \right)}, \quad (22)$$

$$V_{\text{Max}} = \frac{k_2^+ k_1^+ \left(\frac{[\text{H}^+]_o}{K_H} \right)}{k_2^+ \frac{[\text{H}^+]_o}{K_H} \left(1 + \frac{[\text{H}^+]_i}{K_H} \right) + k_1^+ \left(1 + \frac{[\text{H}^+]_o}{K_H} \right)}. \quad (23)$$

The HOE 694 was a kind gift from Dr. U. Albus, Hoescht Aktengesellschaft, Germany.

S.A.N. thanks the Maurice and Phyllis Paykel Trust and the New Zealand Tertiary Education Commission for providing funding. N.P.S. acknowledges support by the Marsden Fund of the Royal Society of New Zealand through grant No. 04-UOA-177 and the National Institute of Health, through NIH/National Institute of Biomedical Imaging and BioEngineering multiscale grant No. RO1-EB005825-01. R.D.V.-J. thanks the British Heart Foundation for funding (grant No. RG/1998012) and the Wellcome Trust (Human Physiome Program grant).

REFERENCES

- Choi, H. S., A. W. Trafford, C. H. Orchard, and D. A. Eisner. 2000. The effect of acidosis on systolic Ca^{2+} and sarcoplasmic reticulum calcium content in isolated rat ventricular myocytes. *J. Physiol.* 529: 661–668.
- Boutrou, C., and R. Vaughan-Jones. 1989. Effect of intracellular and extracellular pH on contraction in isolated, mammalian cardiac muscle. *J. Physiol.* 418:163–187.
- Komukai, K., F. Brette, C. Pascarel, and C. H. Orchard. 2002. Electrophysiological response of rat ventricular myocytes to acidosis. *Am. J. Physiol. Heart Circ. Physiol.* 283:H412–H422.
- Leem, C. H., D. Lagadic-Gossman, and R. D. Vaughan-Jones. 1999. Characterization of intracellular pH regulation in the guinea-pig ventricular myocyte. *J. Physiol.* 517:159–180.
- Poole, R. C., and A. P. Halestrap. 1993. Transport of lactate and other monocarboxylates across mammalian plasma membranes. *Am. J. Physiol. Cell Physiol.* 264:C761–C782.
- Sun, B., C. H. Leem, and R. D. Vaughan-Jones. 1996. Novel chloride-dependent acid loader in the guinea-pig ventricular myocyte: part of a dual acid-loading mechanism. *J. Physiol.* 495:65–82.
- Leem, C. H., and R. D. Vaughan-Jones. 1998. Sarcolemmal mechanisms for pH_i recovery from alkalosis in the guinea-pig ventricular myocyte. *J. Physiol.* 509:487–496.
- Ryan, K. D., R. L. Skolnick, and K. W. Spitzer. 1998. Endothelin-1 stimulates Cl^-/OH^- exchange in ventricular myocytes. *Biophys. J.* 74:A160.
- Leem, C. H. and R. D. Vaughan-Jones. 1997. Chloride-hydroxyl exchange in the guinea-pig ventricular myocyte: no role for bicarbonate. *J. Mol. Cell. Cardiol.* 29:2483–2489.
- Alper, S. L. 2006. Molecular physiology of SLC4 anion exchangers. *Exp. Physiol.* 91:153–161.
- Alvarez, B. V., D. M. Kieller, A. L. Quon, D. Markovich, and J. R. Casey. 2004. SLC26A6: a cardiac chloride-hydroxyl exchanger and predominant chloride-bicarbonate exchanger of the mouse heart. *J. Physiol.* 561:721–734.
- Xie, Q., R. Welch, A. Mercado, M. F. Romero, and D. B. Mount. 2002. Molecular characterization of the murine SLC26A6 anion exchanger: functional comparison with SLC26A1. *Am. J. Physiol.* 283:F826–F838.
- Ko, S. B. H., N. Shcheynikov, J. Y. Choi, X. Luo, K. Ishibashi, P. J. Thomas, J. Y. Kim, K. H. Kim, M. G. Lee, S. Naruse, and S. Muallem. 2002. A molecular mechanism for aberrant CFTR-dependent HCO_3^- transport in cystic fibrosis. *EMBO J.* 21:5662–5672.
- Shcheynikov, N., Y. Wang, M. Park, S. B. H. Ko, M. Dorwart, S. Naruse, P. J. Thomas, and S. Muallem. 2006. Coupling modes and stoichiometry of $\text{Cl}^-/\text{HCO}_3^-$ exchange by SLC26A3 and SLC26A6. *J. Gen. Physiol.* 127:511–524.
- Chernova, M. N., L. Jiang, D. J. Friedman, R. B. Darman, H. Lohi, J. Kere, D. H. Vandorpe, and S. L. Alper. 2005. Functional comparison of mouse SLC26A6 anion exchanger with human SLC26A6 polypeptide variants: differences in anion selectivity, regulation, and electrogenicity. *J. Biol. Chem.* 280:8564–8580.
- Alvarado, F., and M. Vasseur. 1996. Theoretical and experimental discrimination between Cl^-/H^+ symporters and Cl^-/OH^- antiporters. *Am. J. Physiol.* 40:C1612–C1628.
- Lagadic-Gossman, D., K. J. Buckler, and R. D. Vaughan-Jones. 1992. Role of bicarbonate in pH recovery from intracellular acidosis in the guinea-pig ventricular myocyte. *J. Physiol.* 458:361–384.
- Thomas, J. A., R. N. Buchsbaum, A. Zimniak, and E. Racker. 1979. Intracellular pH measurements in Ehrlich ascites tumor-cells utilizing spectroscopic probes generated in situ. *Biochemistry.* 18:2210–2218.
- Kleyman, T. R., and E. J. Cragoe. 1988. Amiloride and its analogs as tools in the study of ion transport. *J. Membr. Biol.* 105:1–21.
- Zaniboni, M., P. Swietach, A. Rossini, T. Yamamoto, K. W. Spitzer, and R. D. Vaughan-Jones. 2003. Intracellular proton mobility and buffering power in cardiac ventricular myocytes from rat, rabbit, and guinea-pig. *Am. J. Physiol.* 285:H1236–H1246.

21. Swietach, P., and R. D. Vaughan-Jones. 2005. Relationship between intracellular pH and proton mobility in rat and guinea-pig ventricular myocytes. *J. Physiol.* 566:793–806.
22. Yamamoto, T., P. Swietach, A. Rossini, S. H. Loh, R. D. Vaughan-Jones, and K. W. Spitzer. 2005. Functional diversity of electrogenic sodium-bicarbonate cotransport in ventricular myocytes from rat, rabbit and guinea-pig. *FASEB J.* 19:A1632.
23. Fozzard, H. A., and C. O. Lee. 1976. Influence of changes in external potassium and chloride ions on membrane potential and intracellular potassium ion activity in rabbit ventricular muscle. *J. Physiol.* 256:663–689.
24. Aronson, P. S., J. Nee, and M. A. Suhm. 1982. Modifier role of internal H^+ in activating the Na^+-H^+ exchanger in renal microvillus membrane-vesicles. *Nature.* 299:161–163.
25. Clemlow, H. F., J. J. Feher, and C. M. Baumgarten. 1992. Modulation of rabbit ventricular cell volume and $Na^+/K^+/2Cl^-$ cotransport by cGMP and atrial natriuretic factor. *J. Gen. Physiol.* 100:89–114.
26. Terashima, K., A. Takeuchi, N. Sarai, S. Matsuoka, E. B. Shim, C. H. Leem, and A. Noma. 2006. Modeling Cl^- homeostasis and volume regulation of the cardiac cell. *Phil. Trans. Roy. Soc. A. Math. Phys. Eng. Sci.* 364:1245–1265.
27. Vaughan-Jones, R. D. 1979. Regulation of chloride in quiescent sheep-heart Purkinje fibers studied using intracellular chloride and pH-sensitive micro-electrodes. *J. Physiol.* 295:111–137.
28. Vaughan-Jones, R. D. 1986. An investigation of chloride-bicarbonate exchange in the sheep cardiac Purkinje fiber. *J. Physiol.* 379:377–406.
29. Carmeliet, E. E. 1961. Chloride ions and the membrane potential of Purkinje fibers. *J. Physiol.* 156:375–388.
30. Swietach, P., C. H. Leem, K. W. Spitzer, and R. D. Vaughan-Jones. 2005. Experimental generation and computational modeling of intracellular pH gradients in cardiac myocytes. *Biophys. J.* 88:3018–3037.
31. van Beaumont, W., J. C. Strand, J. S. Petrofsky, S. G. Hipskind, and J. E. Greenleaf. 1973. Changes in total plasma content of electrolytes and proteins with maximal exercise. *J. Appl. Physiol.* 34:102–106.
32. Vaughan-Jones, R., and K. Spitzer. 2002. Role of bicarbonate in the regulation of intracellular pH in the mammalian ventricular myocyte. *Biochem. Cell Biol.* 80:579–596.
33. Rajendran, V. M., and H. J. Binder. 1993. $Cl^-HCO_3^-$ and Cl^-OH^- exchanges mediate Cl^- uptake in apical membrane-vesicles of rat distal colon. *Am. J. Physiol.* 264:G874–G879.
34. Liedtke, C. M., and U. Hopfer. 1982. Mechanism of Cl^- translocation across small intestinal brush-border membrane. 2. Demonstration of Cl^-OH^- exchange and Cl^- conductance. *Am. J. Physiol.* 242:G272–G280.
35. Jean, T., C. Frelin, P. Vigne, P. Barbry, and M. Lazdunski. 1985. Biochemical properties of the Na^+/H^+ exchange system in rat brain synaptosomes. Interdependence of internal and external pH control of the exchange activity. *J. Biol. Chem.* 260:9678–9684.
36. Wu, M.-L., and R. D. Vaughan-Jones. 1997. Interaction between Na^+ and H^+ ions on Na^+-H^+ exchange in sheep cardiac Purkinje fibers. *J. Mol. Cell. Cardiol.* 29:1131–1140.
37. Liu, D., S. D. Kennedy, and P. A. Knauf. 1996. Source of transport site asymmetry in the Band 3 anion exchange protein determined by NMR measurements of external Cl^- affinity. *Biochemistry.* 35:15228–15235.
38. Stein, W. D. 1986. Transport and Diffusion Across Cell Membranes. Academic Press, San Diego, CA.
39. Papageorgiou, P., B. E. Shmukler, A. K. Stuart-Tilley, L. Jiang, and S. L. Alper. 2001. AE anion exchangers in atrial tumor cells. *Am. J. Physiol.* 280:H937–H945.
40. Knauf, F., C.-L. Yang, R. B. Thomson, S. A. Mentone, G. Giebisch, and P. S. Aronson. 2001. Identification of a chloride-formate exchanger expressed on the brush border membrane of renal proximal tubule cells. *Proc. Natl. Acad. Sci. USA.* 98:9425–9430.
41. Waldegger, S., I. Moschen, A. Ramirez, R. J. H. Smith, H. Ayadi, F. Lang, and C. Kubisch. 2001. Cloning and characterization of SLC26A6, a novel member of the solute carrier 26 gene family. *Genomics.* 72:43–50.
42. Vaughan-Jones, R. D., and M. L. Wu. 1990. Extracellular H^+ inactivation of Na^+-H^+ exchange in the sheep cardiac Purkinje fiber. *J. Physiol.* 428:441–466.
43. Green, J., D. T. Yamaguchi, C. R. Kleeman, and S. Muallem. 1988. Cytosolic pH regulation in osteoblasts. Interaction of Na^+ and H^+ with the extracellular and intracellular faces of the Na^+/H^+ exchanger. *J. Gen. Physiol.* 92:239–261.
44. Wakabayashi, S., T. Hisamitsu, T. X. Pang, and M. Shigekawa. 2003. Kinetic dissection of two distinct proton binding sites in Na^+/H^+ exchangers by measurement of reverse mode reaction. *J. Biol. Chem.* 278:43580–43585.
45. Lacroix, J., M. Poet, C. Maehrel, and L. Counillon. 2004. A mechanism for the activation of the Na^+/H^+ exchanger NHE-1 by cytoplasmic acidification and mitogens. *EMBO Rep.* 5:91–96.
46. Smith, N. P., and E. J. Crampin. 2004. Development of models of active ion transport for whole-cell modeling: cardiac sodium-potassium pump as a case study. *Prog. Biophys. Mol. Biol.* 85:387–405.